SIMULATIONS OF PRESENT-DAY AND FUTURE CLIMATE OVER SOUTHERN AFRICA USING HadAM3H

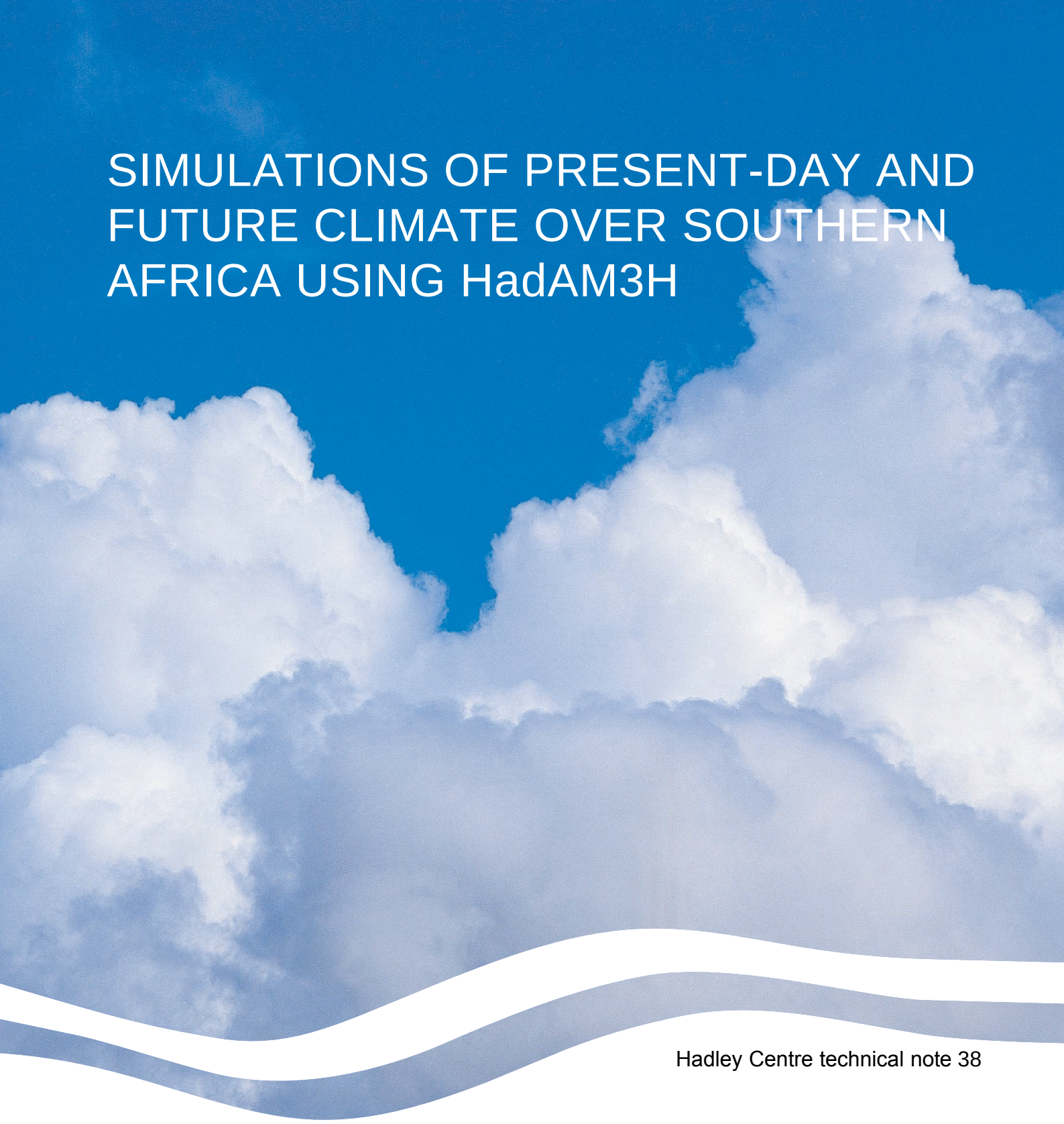

Hadley Centre technical note 38

D. A. HUDSON and R.G. JONES

13 August 2002

Met Office

SIMULATIONS OF PRESENT-DAY AND FUTURE CLIMATE OVER SOUTHERN AFRICA USING HadAM3H

D. A. HUDSON and R.G. JONES

Met Office, Hadley Centre for Climate Prediction and Research, London Road, Bracknell, RG12 2SY, U.K.

ABSTRACT

A high resolution (~150 km) GCM, HadAM3H, is used to obtain enhanced regional information from a fully coupled atmosphere-ocean GCM, HadCM3, in time-slice experiments of the periods 1961-90 and 2071-2100. For the future scenarios, the IPCC SRES A2 and B2 emissions scenarios have been used, and the model results of present-day and future climates are analysed over southern Africa. The model is generally able to capture the circulation dynamics of the present-day climate, reproducing the primary features of observed circulation and the general pattern of seasonal change. In summer, however, convergence into the Intertropical Convergence Zone and Zaire Air Boundary is too strong, resulting in a positive rainfall bias over much of southern Africa. In addition, there is a surface temperature cold bias over much of the land, which is related to an excess of thick cloud and less incoming solar radiation reaching the earth's surface, as well as the possibility of greater evaporative cooling in the model. In winter, surface temperatures south of 30°S are colder than observed, whereas between 10°S and 25°S there is a warm bias. These biases are related to cloud and circulation anomalies. In the climate change experiments, the weaker forcing in the B2 scenario results in intermediate values of surface temperature compared to the controls and the A2 scenario, with the results being less clear for precipitation. The A2 future scenario over southern Africa suggests an average warming over the region of 3.9°C in summer and 4.1°C in winter. There tends to be a drying over western and central tropical and subtropical land areas in summer, whereas equatorial regions tend to become wetter, with more intense and extreme rainfall. The same is true in general for equatorial regions in winter, but over the South Western Cape winter rainfall region of South Africa, there is a reduction in mean seasonal rain and a tendency for extreme rainfall events to become less likely.

1. INTRODUCTION

Southern Africa experiences a highly variable climate and presents significant vulnerabilities in the face of probable human-induced climate change. Apart from highly variable rainfall and water being a limited resource in many countries, the subcontinent is generally characterised by high population growth rates, a reliance in many areas on subsistence level agriculture, generally low levels of income, and high population densities on marginal lands. It is essential that we acquire knowledge of possible future climate changes, so as to facilitate planning for the next five to ten decades. In order to be able to adapt and respond to the possible impacts of climate change, there needs to be extensive research into the consequences of climate change, not only at global and hemispheric scales, but also at regional and local scales, where the impacts will be felt.

Although numerical model simulations using global general circulation models (GCMs) are the most appropriate tools for addressing questions related to future climate changes, the typical grid resolution is such that the complex regional precipitation and temperature patterns over the African sub-continent are often not captured. In addition, in order to formulate adaptation policies in response to climate change impacts, reliable climate change information is required at finer spatial scales than that of a typical GCM grid-cell. Unfortunately, the skill level (von Storch *et al*., 1993) of GCMs is usually poor at the scale of the grid cell, but increases as results are averaged over a

larger grid, such that simulations are reasonably accurate at synoptic scales and larger (Hewitson and Crane, 1996).

The resolution of a fully-coupled atmosphere-ocean GCM is limited in part by the computational expense of running the century-long simulations that are required to adequately integrate the climate system for climate change studies. However, one method of obtaining enhanced regional information from fully coupled GCMs is to use higher resolution atmosphere-only GCMs to model specific periods of interest from the coupled GCM transient simulation, in what has been referred to as "time-slice" experiments.

The resolution of the Hadley Centre's fully-coupled atmosphere-ocean GCM, HadCM3, is 3.75° latitude by 2.5° longitude. In the present study, selected boundary forcing from HadCM3 is used to drive a high resolution (~150 km) atmosphere-only GCM, HadAM3H, over two time periods, namely 1961-90 and 2071-2100. These simulations provide finer spatial and temporal detail than the corresponding HadCM3 simulations. The present study examines the GCM (HadAM3H) simulations of present-day and future climates over southern Africa.

2. MODEL DESCRIPTION AND EXPERIMENTAL DESIGN

HadAM3H is an atmosphere-only model which has been derived from the atmospheric component of HadCM3 (Gordon *et al*., 2000; Pope *et al*., 2000), the Hadley Centre's state of the art coupled model. The horizontal resolution of HadAM3H is 1.24° latitude × 1.88° longitude, and has 19 layers in the vertical which are based on a hybrid vertical coordinate system (Simmons and Burridge, 1981). The model employs spherical polar coordinates on a regular latitude-longitude grid and has a 15 minute timestep. The development of HadAM3H, together with a full description of the model, is provided by Jones *et al*. (1999) and Murphy *et al*. (2002).

The high resolution atmosphere-only GCM is used to obtain an improved regional-level simulation over specific periods of interest identified from the coupled model integration. Two periods or time slices, namely 1961-90 and 2071-2100, have been selected from transient simulations (1860-2100) with HadCM3. These HadCM3 experiments are documented by Johns *et al*. (2001). Observed time-dependent fields of sea-surface temperature (SST) and sea-ice (HadISST1 dataset, Rayner *et al*, 2002) are used as lower boundary conditions in the control simulation with HadAM3H. In the climate change experiments, the HadCM3 SST anomaly is added to the observed data to use as the lower boundary forcing. Time-dependent greenhouse gas and anthropogenic sulphate emissions are the same as in the corresponding HadCM3 time slice, and initial atmospheric and land surface conditions are interpolated from HadCM3. HadAM3H is favoured over HadCM3 for deriving regional climate information and driving regional models, since it has a higher resolution (150 km versus about 300 km) and exhibits an improved control climate, especially with respect to the positioning of the storm tracks of the Northern Hemisphere (Jones *et al*., 1999; Murphy *et al*., 2002). The representation of clouds and condensation, and the impact of land-surface physics on surface temperatures are also substantially improved (Jones *et al*., 1999; Murphy *et al*., 2002).

An ensemble of three HadAM3H runs for the period 1961-1990 have been performed. The climate change simulations (2071-2100) are based on the IPCC (Intergovernmental Panel on Climate Change) A2 and B2 SRES scenarios. The IPCC SRES scenarios provide a range of scenarios of future greenhouse gas and sulphur emissions based on a number of assumptions in driving forces, for example technological, demographic and socio-economic developments (IPCC, 2000). These scenarios have been used in the production of the IPCC Third Assessment Report on climate change (IPCC, 2001). The A2 scenario assumes a higher population growth rate than the B2 scenario, and slower per capita economic growth rates and technological change. As a result, the A2 scenario has a larger growth rate and higher emissions of CO_2, as well as larger emissions of methane, nitrous

oxides and HFCs (hydro-fluoro carbons). For more details of these emission scenarios, refer to the IPCC special report on emission scenarios (IPCC, 2000). An ensemble of three simulations has been run for the A2 scenario, and one simulation for the B2 scenario.

3. OBSERVED DATA

For the assessment of model performance, several datasets have been used. Extensive use is made of the ECMWF reanalysis data (hereafter referred to as ERA) (Gibson *et al*., 1997). The data are presented on a 2.5° × 2.5° grid and extend from 1979 to 1993. Precipitation and 1.5 m temperatures over southern Africa are compared to the global 0.5° × 0.5° resolution CRU (Climatic Research Unit) climatology for the time period 1961 to 1990 (New *et al*., 1999). Precipitation is also evaluated against the CMAP precipitation analysis (Xie and Arkin, 1997). This 2.5° × 2.5° global dataset extends from 1979 to 1999 and is derived from satellite observations and rain gauge estimates. In order to assess the validity of daily precipitation statistics and extremes, precipitation data on a 0.25° grid over South Africa have been used. These daily data extend from 1950-1997 and have been produced in gridded format by the Climate Systems Analysis Group (Department of Environmental and Geographical Science) at the University of Cape Town from station data obtained from the South African Computer Centre for Water Research (CCWR). For comparison with the GCM daily data, the observed daily precipitation data are aggregated to the scale of the GCM by averaging observed grid box values over appropriate corresponding GCM grid boxes. The model's radiation fluxes are compared with satellite derived data from the Earth Radiation Budget Experiment, ERBE (Harrison *et al*., 1990), extending from 1985 to 1990 and produced on a 2.5° × 2.5° grid. Model cloud amounts are compared with the 2.5° × 2.5° data from the International Satellite Cloud Climatology Project, ISCCP (Rossow and Shiffer, 1991), for the period 1989 to 1993.

4. CONTROL CLIMATE

The reliability of a GCM climate change simulation is dependent in part on the atmospheric processes governing the control climate of the GCM. Hence, it is essential to have a good understanding of how HadAM3H performs over southern Africa.

4.1. Mean Fields

Rainfall over most of southern Africa is markedly seasonal (except for the south coast, the arid south-west and the moist tropics), with more than 80 % of rain falling in the summer half of the year (October to March) (Hobbs *et al*., 1998). Summer (DJF) is characterised by a complex interplay of converging airstreams which produce the Intertropical Convergence Zone (ITCZ) over the eastern half of the subcontinent and the Zaire Air Boundary (ZAB) over western parts (southern Angola and Botswana). The three primary converging airstreams are the north-east airflow from the East African monsoon, which crosses the equator and moves into eastern Africa and southwards; tropical easterlies from the Indian Ocean and the low-level recurved westerlies that enter southern Africa from the Atlantic Ocean at about 12°S. The convergence of these major airstreams facilitates vertical motion, and tropical lows and troughs tend to form preferentially on a daily basis in these dynamic convergence zones. It is a challenge to any climate model to be able to accurately simulate such complex circulation. The seasonal mean positions of the ITCZ and the ZAB mark regions of maximum rainfall over the subcontinent, and slight shifts in these positions in a model can dramatically alter the climate of a particular region.

HadAM3H simulates the large scale spatial features of the summer circulation reasonably well, although there are a number of systematic biases. As has been found with other Hadley Center models (Stratton, 1999; Pope *et al*., 2000), there is a low pressure bias in the tropics in summer, and

this is also the case over southern Africa in HadAM3H (Figure 1). The sea level pressure field over the land exhibits deviations of up to 6 hPa compared to observed (Figure 1). However, the magnitude of these results should be treated with caution, since much of the region lies above 1000 m and mean sea level pressure will depend strongly on the model's orography and the method used to interpolate surface pressure to sea level. In fact, all the grid points that show maximum negative sea level pressure anomalies are located in mountainous regions. Notwithstanding, the 850 hPa (Figure 2) and 700 hPa fields (not shown) also display negative geopotential height anomalies over southern Africa. The general negative pressure bias appears to be a result of enhanced convergence in the ITCZ and ZAB and is associated with increased ascent around 15°S and enhanced Hadley and Walker circulations in the model compared to observed. In HadAM3H, the shallow equatorial westerlies from the Atlantic Ocean are stronger, deeper and more extensive than observed; and the north-east airflow from the East African monsoon and the easterly trade winds off the Indian Ocean are also stronger (Figure 2). In addition, these three airstreams represent important moisture feeds for the subcontinent, therefore in the model the associated moisture fluxes over the land increase (not shown), causing increased moisture convergence over the subcontinent. Consequently, although the model captures the general pattern of rainfall over the subcontinent, the magnitude of rainfall is overestimated, especially south of 10°S over the central N-S axis of the region (greater than 2 mm/day difference) (Figure 3). In addition, upper tropospheric divergence (not shown) in the model extends southwards in a NW-SE axis over South Africa, whereas in the observed data there are weak convergence fields over the country. This divergence anomaly is associated with the positioning and strength of the upper level Atlantic westerly wave and the upper level ridge over southern Africa. In the model, upper level circulation over South Africa and the adjacent Atlantic Ocean is more meridional (not shown), such that South Africa is influenced by stronger divergence ahead of the trough axis. This could contribute to the fact that the GCM is not good at simulating the tight east-west gradient of rainfall that is observed over South Africa, with too much rainfall being simulated over the arid western areas.

There are, however, three primary regions where the model is drier than observed, namely over the north-west coast of the subcontinent (between about 0° and 10°S), over the east coast south of Lake Malawi (i.e. southern Malawi, Mozambique and northern Zimbabwe), and over Madagascar (Figure 3). For the latter two regions, this appears to be related to the slight northward displacement of the ITCZ in the model, which lies near these regions in the observed data. In addition, south of Lake Malawi, the south-east trades are stronger than observed and thus contribute to a near-surface divergence anomaly and result in the zone of preferential convergence occurring further northwards. Over the NW coast the dry anomaly may be related to stronger low level recurved westerlies, which cause a near-surface divergence anomaly in this region and reduce the potential for uplift and rainfall.

The representation of clouds has long been known to be a source of error and uncertainty in GCM simulations. In general, over the southern African region HadAM3H tends to simulate too much cloud at low, middle and upper tropospheric levels, especially thick cloud (optical thickness > 25; as defined in the ISCCP data (Rossow and Shiffer, 1991)) (Figure 4). Thick cloud affects the attenuation of shortwave radiation, and in the model, larger amounts of thick cloud result in a reduction in the amount of shortwave radiation reaching the earth's surface compared to observed over much of southern Africa south of 10°S (shortwave cloud forcing is increased, i.e. negative values in Figure 4).

As observed, the model summer surface (1.5 m) air temperature field shows a warm western interior which is also arid. However, it underestimates the extent of this warm and arid region. There is actually a surface temperature cold bias over most of southern Africa in the model, of up to 4°C in some regions (Figure 4). This bias may be a result of two different processes. Firstly, as mentioned above, more thick cloud in the model means that there is less incoming solar radiation

reaching the earth's surface (not shown). Secondly, over the south-western region (primarily west of 25°E and south of 20°S) there may be greater evaporative cooling at the surface of the earth as a result of the excess precipitation in the model. In this region the model soil moisture content at the beginning of summer is low (in winter the soils dry out such that soil moisture is generally less than 40 cm, but with extensive areas less than 10 cm), thus most of the soil moisture and evaporation that occurs during summer comes from the rainfall that falls in summer (model P-E values are generally less than ±1 mm/day). A comparison of the model-derived evaporation with observed summer precipitation shows that evaporation from the model exceeds observed precipitation south of ~15°S (by up to 4 mm/day). This suggests that the model evaporation is greater than observed evaporation over these moisture limited regions, leading to greater evaporative cooling.

The model is generally better at simulating the climate of southern Africa during winter (JJA) compared to summer. There are, however, still significant biases. With the northward movement of the ITCZ in winter, most of southern Africa is dry. The subcontinent is dominated by a high pressure system and general subsidence and stability prevail. The only regions in southern Africa experiencing any significant rainfall in winter are the northern region of the Democratic Republic of Congo, the east coast of Madagascar and the southern and south-west coasts of South Africa. With the equatorward expansion of the midlatitude westerlies, the south and south-west coasts of South Africa receive rainfall associated with the passage of westerly waves and their attendant cold fronts.

As for summer, pressures in the GCM are too low over the land and the continental high pressure is not as well defined in the model (Figure 5). At the 700 hPa level in the observed data there is a clear ridge at about 20°S connecting the South Atlantic and South Indian high pressure systems, whereas in the model over the western part of the land and adjacent Atlantic Ocean this ridge axis is displaced northwards due to stronger meridional circulation and a stronger trough over the Atlantic Ocean compared to observed (Figure 5). In addition, the cross-equatorial jet off the coast of eastern Africa which flows into the Asian summer monsoon is too strong (Figure 5).

Model seasonal mean surface air temperatures compare well with the CRU climatology in terms of the large scale spatial features. However, south of about 30°S, over South Africa, surface temperatures in the model tend to be colder than observed (by about 2°C) (Figure 6). This is probably related to the larger amounts of thick cloud in the model and the resulting reduction in shortwave radiation reaching the earth's surface (Figure 6). Between about 10°S and 25°S over the land, there is a surface warm bias (up to 4°C) (Figure 6). This does not extend into the upper troposphere, instead being replaced by a cold bias (up to 2°C) at the 500 hPa level (not shown). The surface warming probably results from a combination of anomalous advection from the north, and an overestimation of shortwave radiation reaching the surface, since the model generally has less total cloud (not shown) than observed over this region.

There are few differences in precipitation between the model and observed in winter. The GCM tends to be too dry over the land near 5°N and over the north and south coasts of Madagascar (Figure 7). Madagascar has a tendency to be too dry in both summer and winter, and this may be related to the smoothed orography in the model compared to observed resulting in reduced topographical forcing.

The seasonal cycle of sea level pressure, surface (1.5 m) temperature and precipitation have been analysed for 8 southern African "stations" (the same stations as chosen by Nicholson *et al.*, 1988). The values from the nearest gridbox to each station location for the GCM and gridded observed data have been used. The seasonal cycle of sea level pressure is fairly well represented at all stations, except that, as previously mentioned, there is a negative pressure bias in all seasons and at all stations in the model (Figure 8). The bias is largest in spring and summer, and smallest in the winter, especially for the four stations that are positioned nearest to the ITCZ/ZAB in summer

(Songea, Lubumbashi, Harare and Tsumeb). These anomalies imply that there is a more rapid arrival (withdrawal) of the ITCZ going from winter (summer) to summer (winter) in the model compared to observed.

In terms of the seasonal cycle of surface temperature, stations north of 26°S show early summer temperatures that are too warm in the model and mid/late summer temperatures that are too cold (Figure 9). It has been mentioned previously that the mid-summer negative temperature bias is probably due to an excessive latent heat flux, as well as an excess of thick cloud in the model, resulting in a reduction in shortwave radiation reaching the earth's surface. Most of these stations experience very little rainfall in October compared to January, and cloud cover and latent heat fluxes are lower, thus the model error associated with these feedbacks is unlikely to have a large effect in October, but is manifest from November onwards through the wet season by the marked drop in surface temperatures. For the three stations south of 25°S (Port Elizabeth, Okiep and Cape Town), the model provides a good representation of the seasonal cycle, perhaps with a slight tendency to be too cool in winter (as was shown with the seasonal mean field).

The overestimation of summer rainfall is seen in the seasonal cycles of all the summer rainfall stations (Figure 10), with the exception of Harare (as described previously). In the model the eastern African stations of Songea, Lubumbashi and Harare have too little rainfall in the autumn months. Lubumbashi and Tsumeb exhibit an earlier onset of rainfall in spring/summer, probably associated with the earlier arrival of the ITCZ in this area. Pope *et al*. (2000) found a similar result with HadAM3 (the atmospheric component of HadCM3), in that there was a tendency for the seasonal shifts in tropical rainfall over Africa and Asia to occur earlier and to be more marked than observed, leading to errors in the transition seasons. The observed second peak of rainfall at Songea during April is not captured by the model. Port Elizabeth, on the south coast of South Africa, receives rainfall all year round, but this is not exhibited by the model which simulates a seasonal cycle with maximum rainfall in summer. In summer, this region receives rainfall from troughs in the tropical easterlies and ridging anticyclones. When the South Atlantic High Pressure is centred to the south or south-west of South Africa, then ridging over the land can cause rainfall over southern and eastern coastal areas. It has already been shown that the tropical easterly wave trough is deeper than observed in the model, but in addition, there are anticyclonic anomalies south and south-west of South Africa (Figure 2), suggesting that ridging anticyclones may be more prevalent in the model. This combination of circulation anomalies may explain the overestimation of summer rainfall over Port Elizabeth. In contrast, in winter the region receives its rainfall from midlatitude cyclones and their attendant cold fronts. The 700 hPa wind and geopotential height field show that there is an anticyclonic anomaly over the Indian ocean south of Madagascar in the model (Figure 5). It is thus possible that storms are being steered preferentially south-eastwards by this blocking effect, perhaps contributing to the underestimation of winter rainfall over Port Elizabeth in the model. The model simulates the winter rainfall peak in Cape Town, but winter rainfall is less than observed and tends to reach its peak later in the winter season. The former may be due in part to insufficient orographic forcing in the model.

The representation of the southern hemisphere seasonally averaged quasi-stationary wave numbers 1 and 3 have been analysed by means of Fourier analysis of the 500 hPa heights along latitude circles. Waves 1 and 3 both have an important influence on the weather of southern Africa (Tyson and Preston-Whyte, 2000). The results show that HadAM3H adequately captures the amplitude and phase of these quasi-stationary long waves.

4.2. Variability

It is important that the model be able to reproduce aspects of variability in the climate system, and not only average features. The observed mean intraseasonal variability of sea level pressure (the

standard deviation of daily values from the respective seasonal mean pressure) is largest over the midlatitude ocean and decreases towards the tropics (Figure 11). The model represents this pattern well, with the largest errors (less than 2 hPa) being over the Indian Ocean east of Madagascar. Variability increases in winter over midlatitude and subtropical regions, which again the model adequately captures (Figure 11).

The interannual variability of the seasonal mean sea level pressure is also largest in the midlatitudes and decreases towards the tropics, and is larger in winter (Figure 12). HadAM3H simulates this general pattern relatively well. In summer, there is a tendency for too much year-to-year variation east of Madagascar, and too little variability over the arid south western region of South Africa (Figure 12). Over the land in winter, there is slightly too much variability over central regions around 20°S, and too little around 10°S over central and western regions (Figure 12).

Interannual variability of seasonal mean precipitation has been analysed over southern Africa (land points only) for summer and winter. Overall, the GCM performs quite well, and captures the general pattern in both seasons. In winter, in those areas that receive rainfall during this season, there is a tendency for less variability in the GCM (Figure 13). These results are reproduced in Figure 14. Here the 30-year mean and standard deviations of seasonal precipitation totals over land areas are displayed for the three simulations constituting the HadAM3H control ensemble, as well as the CRU observed data. The data are represented as spatial averages over 6 regions in southern Africa (three zones, referred to as the subtropical, tropical and equatorial zones, divided into western and eastern sections, with 24°E as the dividing meridian). It is clear that in summer and winter there is a large degree of coherence, in terms of both the mean and standard deviation, between the replicates of the HadAM3H ensemble. As was displayed in Figure 13, the model performs well in capturing the observed rainfall variability, notably the relatively large interannual variability in the western and eastern subtropical regions in winter. The previously shown overestimation of summer rainfall by the model is clear in the western subtropical, western tropical, eastern subtropical and eastern equatorial regions.

The validation of GCM daily precipitation data is limited by the lack of reliable observed data sets, a particular problem for vast areas of Africa. As such, in this study the validation is restricted to South Africa, for which daily data are available. A comparison of the simulated average number of rain-days (days with more than 0.2 mm of rain) with observations over South Africa (aggregated to the GCM scale) shows that the model tends to overestimate the number of rain-days in summer, especially over central and western regions of South Africa, such that the sharp east-west gradient is not as well defined in the model (Figure 15). The simulated intensity (rain per rain-day) of summer rainfall is also overestimated. In contrast, in winter the model seems to closely reproduce the number of rain-days over South Africa, but underestimates the intensity of rainfall in coastal regions (Figure 16). This may be related to the horizontal resolution of the model such that there may be insufficient topographical forcing and dynamical uplift associated with the steep escarpment near the coast.

In the fields of hydrology and civil engineering, a common means of examining extreme rainfall is in terms of return periods. For example, structures such as bridges and dams are designed to withstand the largest precipitation event anticipated within a particular period (e.g. the one in 20-year flood event). This aspect of extreme rainfall is investigated in the present study by fitting Generalised Extreme Value (GEV) distributions to samples of seasonal precipitation maxima (obtained from daily data) at each grid box. The procedure follows the method outlined by Kharin and Zwiers (2000). The GEV distribution is given by:

$$F(x)=\begin{cases}\exp\{-[1-k(x-\xi)/\alpha]^{1/k}\}, & k<0, \quad x>\xi+\alpha/k,\\ \exp\{-\exp[-(x-\xi)/\alpha]\}, & k=0,\\ \exp\{-[1-k(x-\xi)/\alpha]^{1/k}\}, & k>0, \quad x<\xi+\alpha/k,\end{cases}$$

where ξ, k and α are the adjustable scale parameters describing the distribution's location, shape and scale respectively. After these parameters have been estimated for each grid box, using the method of L-moments (Hosking, 1990; Kharin and Zwiers, 2000, including using hybrid estimators when the method of L-moments produces non-feasible parameter estimates, as described by Kharin and Zwiers), the T-year return value is obtained using:

$$\hat{X}_{RV_T}=\begin{cases}\hat{\xi}+\hat{\alpha}\{1-[-\ln(1-1/T)]^{-\hat{k}}\}/\hat{k}, & \hat{k}\neq 0,\\ \hat{\xi}-\hat{\alpha}\ln[-\ln(1-1/T)], & \hat{k}=0.\end{cases}$$

In the present study, precipitation values ($\hat{X}_{RV_T}$) associated with a return period (T) of 20 years are examined. These values are thresholds that (according to the fitted distribution) will be exceeded once every 20-years (the 20-year return value corresponds to the value on the x-axis of a probability density function such that the area under the right-hand tail of the distribution is 0.05). Estimated 20-year return values of daily precipitation from the GCM and from the CCWR observed data (aggregated to the GCM-scale) over South Africa are displayed in Figure 17. In general, the model simulates plausible return values over South Africa. However, consistent with previous results, values tend to be too large in summer, and too low over coastal regions in winter. As mentioned previously, this underestimation in coastal regions may be associated with smoothed topographical fields in the model, since the interaction between atmospheric circulation and topography is important in these regions.

Distributions of daily rainfall are examined for three land regions over South Africa: the east coast (35°S-20°S, 30°E-35°E), the eastern interior (30°S-25°S, 25°E-30°E), and the south western Cape (35°S-30°S, 15°E-20°E) (the land areas of the three boxes marked on Figure 17, and only using grid boxes for which the observed data are defined). It is important to note that the area of these land regions is not the same, therefore the resulting area-averaged histograms are subject to varying degrees of smoothing. In general the model performs relatively well in capturing the shape of the rainfall distributions (Figure 18). Over the east coast and eastern interior of South Africa in summer, the overestimation of precipitation seen in the seasonal mean field (Figure 3) is related to higher rainfall in the medium to high rainfall intensity classes. Over the south western Cape the most extreme precipitation is slightly underestimated. In winter, the finding that the model tends to underestimate the 20-year return values (Figure 17) is borne out by the distributions for the east coast and south western Cape (Figure 18).

In summary, although there are important systematic errors in certain variables, most of the large scale spatial features of the seasonal circulation over southern Africa are reasonably represented by the model. The analysis indicates that with due care, HadAM3H can be used to study the physical processes underlying the general circulation over the region, and to provide indications of possible future climate scenarios.

5. FUTURE CLIMATE

5.1. Mean Changes

Tables 1 and 2 show the spatially averaged (over land points only) summer and winter temperature and precipitation results for the control, A2 and B2 simulations. The A2 future scenario over

southern Africa suggests an average surface warming over the region of 3.9°C in summer and 4.1°C in winter (derived from Table 1). As one might expect, due to the weaker emission forcing in the B2 scenario compared to the A2 scenario, the temperature increase relative to the controls is smaller in the B2 simulations (2.7°C in summer and 2.8°C in winter) (derived from Table 1). This is also clear in the plots of seasonally varying temperature (Figure 19), which are averaged over the same six land regions mentioned in section 4.2 above. This suggests a linear response of temperature to the different forcing scenarios. However, the results for precipitation are perhaps more complicated. The seasonal cycles for the western equatorial and western tropical regions suggest a linear response, but this is not as clear for the other regions (Figure 20). In addition, for precipitation it is evident that there is a larger degree of variability between simulations within an ensemble (i.e. for the control and A2 scenario respectively) compared to temperature (Figures 19 and 20). Nonetheless, in terms of the seasonal mean fields, the spatial correlations between the members of the ensemble for both temperature and precipitation respectively and in both seasons do not fall below 0.9 indicating that there is a high degree of coherence between the simulations within an ensemble. In addition, there are high correlations between the pattern of change from the A2 scenario and the B2 scenario for both temperature and precipitation (no correlations below 0.8). The results suggest that intra-ensemble variability is not a significant factor at the level of the long-term seasonal mean. Subsequent discussion in this report will focus on the results from the A2 scenario, since there is a larger signal-to-noise ratio compared to the B2 scenario.

In response to the A2 emissions scenario forcing, temperatures increase throughout the troposphere in the southern African domain in both summer and winter (Figure 21). Predicted warming is greater in the upper troposphere over tropical and equatorial latitudes. The surface temperature response is larger over the land than the adjacent oceans (Figure 22), and may be a result of less evaporative heat loss over the land compared to the oceans, as well as the greater thermal inertia of the oceans. In summer, the surface temperature increase over the land is largest (about 5°C) over the western half of the subcontinent, and smallest (about 3°C) in the vicinity of Kenya and Tanzania (Figure 22). A moderated but similar pattern of change can be seen from the B2 scenario results (Figure 22), corroborating the aforementioned idea of a linear response to the forcing scenarios. Results from the A2 scenario simulations suggest that the temperature anomaly patterns are largely the result of cloud and latent heat flux feedbacks. Over Kenya and Tanzania the smaller temperature increase may be the result of a negative feedback induced by increased cloudiness (of thick cloud especially) (Figure 23), causing an increase in shortwave cloud forcing (Figure 24) and a reduction in insolation reaching the earth's surface. In addition, there is an increase in the surface moisture flux in this region (Figure 25), which would result in greater evaporative cooling. In contrast, over the western half of the subcontinent the temperature increase is enhanced by a positive feedback resulting from a reduction in thick cloud cover (Figure 23) and shortwave cloud forcing (Figure 24), causing an increase in shortwave radiation reaching the earth's surface. The temperature increase is also enhanced by the reduced surface moisture flux in this region (Figure 25) resulting in less evaporative cooling.

In winter, the largest warming (about 6.5°C in the A2 scenario and about 4°C in the B2 scenario) over the subcontinent is found over the Democratic Republic of Congo (Figure 22). The A2 scenario results show that the warming has been enhanced in this region due to a reduction in thick cloud amount (Figure 23), shortwave cloud forcing (Figure 24), and evaporative cooling (Figure 25).

HadAM3H simulates sea level pressure decreases over the subcontinent in summer and winter for the A2 scenario, with largest decreases (up to 2 hPa) occurring south of 20°S (Figure 26). A similar pattern of change is found for the B2 scenario (Figure 26), but the magnitude of change suggests that sea level pressure may exhibit a non-linear response to the forcing scenarios. The A2 scenario results show that the pressure decrease over the land is a shallow effect, probably due to the effects

of surface heating, and does not imply a strengthening of the tropical easterly wave trough. At the 850 hPa level, geopotential height changes indicate increases in heights over southern Africa in both summer and winter (Figure 27). There is also an increase in the geopotential heights of the 500 hPa and 300 hPa surfaces over southern Africa (not shown), which is what we might expect with a general warming of the atmospheric column.

In summer, there is a tendency for a decrease in rainfall south of about 10°S, but with statistically significant decreases over western and central land areas and largest changes being between about 10°S and 20°S over northern Namibia and southern Angola (the 2 mm/day reduction translates to about a 20-30% reduction in rainfall) (Figure 28). In contrast, there is a statistically significant increase in rainfall north of 10°S and east of 20°E (Figure 28). For the land regions which experience rainfall during winter, namely the south western Cape of South Africa and equatorial regions, there is a statistically significant increase in winter rainfall over central equatorial longitudes (~1 to 2 mm/day or 20 to 30%), and statistically significant decreases over western equatorial longitudes (~30% reduction) and the south western Cape (~10 to 20% reduction) (Figure 28). Large regions of the rest of southern Africa also exhibit statistically significant decreases in rainfall (Figure 28), although it must be remembered that most of these regions actually receive very little winter rainfall as it is. The B2 scenario results show similar patterns of change to the A2 scenario (Figure 29), but it is not clear that precipitation scales in the same way as temperature. Like sea level pressure, the response of precipitation to the scenario forcing may be non-linear.

The general increase in rainfall over equatorial latitudes (0°S to 10°S), particularly in summer, may be a result of enhanced convection under future conditions. The warming of the atmosphere leads to an increase in specific humidity, especially over equatorial regions (Figure 30), and this in turn contributes to enhanced low level moisture convergence in this region. These increases in precipitation are generally associated with increases in the root-zone soil moisture content (Figure 31), and evaporation (except west of 25°E in summer) (Figure 25).

The general reduction in rainfall over the land south of about 10°S in summer (Figure 28), and particularly over western regions, is associated with a general reduction in thick cloud cover (Figure 23), a reduction in the root-zone soil moisture content (Figure 31) and a general reduction in evaporation (Figure 25). The zonally averaged cross-section of vertical velocities shows that between about 10°S and 25°S there is increased subsidence in the troposphere, especially at mid-tropospheric levels (not shown). In addition, at the 500 hPa level, there is an anticyclonic anomaly in the circulation field, centred over western regions of southern Africa south of about 10°S (not shown). At the 850 hPa level the geopotential height changes indicate a strengthening of the South Atlantic and South Indian High Pressures and a reduction in strength of the tropical low (centred over southern Angola and northern Namibia) and easterly wave (Figure 27). These circulation changes may contribute to the reduction in rainfall over southern Africa.

It is important to remember that biases in the model control climate (mentioned in section 4) may distort the climate change signal. For example, the above-mentioned reduction in rainfall over the south-west of the sub-continent is associated with a reduction in evaporation, and thus an enhanced warming over the region. Western areas of South Africa, Namibia and southern Angola receive less than 2 mm/day under present-day conditions in summer. However, the model simulates too much rainfall over this region (sometimes exhibiting a positive bias of more than 2 mm/day) (Figure 3), and the rainfall reductions that are predicted under climate change are up to 2 mm/day (Figure 28). Thus, the warming that is simulated under climate change conditions (Figure 22) may be exaggerated in certain of these areas, due to the excessive latent heat fluxes that exist in the model.

An examination of the changes in rainfall seasonality has been undertaken for the 8 southern African stations mentioned in section 4.1 (Figure 32). Songea, Lubumbashi and Harare, the three

stations situated furthest north and east, show very little change in rainfall seasonality, although Lubumbashi does exhibit reduced late summer (January and February) rainfall in the future scenario. The summer drying over southern Africa can be seen in the seasonal cycles of Tsumeb, Johannesburg and Okiep, and occurs predominantly in the latter half of the summer season. There do not seem to be any major shifts in seasonality, except for Port Elizabeth. Port Elizabeth experiences all-year round rainfall, which is not reflected by the model, therefore predictions of changes to precipitation seasonality in this region must be treated with caution. Cape Town experiences a reduction in mid-winter rainfall.

5.2. Variability

Much of southern Africa experiences a high degree of intra- and interannual rainfall variability, and the region is particularly vulnerable to floods and droughts. In addition, it is the changes to variability and extremes that have a direct effect upon society, rather than the mean changes.

In summer in response to the A2 scenario forcing, there is a decrease in the interannual variability of seasonal mean precipitation over western tropical and subtropical land areas, but an increase in variability west of Lake Tanganyika in the Democratic Republic of Congo (Figure 33). In winter, over most of Africa south of the equator there is a reduction in the interannual variability of seasonal mean precipitation (Figure 33).

Analysis of daily precipitation shows that in summer there is a general reduction in the number of rain-days (days with more than 0.2 mm of rain) over southern Africa (Figure 34). However, there are key regions where the average intensity of rainfall (rain per rain-day) increases (Figure 34). In fact, the increase in rainfall over equatorial latitudes (0°S to 10°S) that is seen in the mean field (Figure 28) is related to an increase in the intensity of rainfall rather than a change in the number of rain-days (Figure 34). In contrast, the decrease in mean summer rainfall over western and central land areas south of about 10°S (Figure 28), is related to a decrease in the number of rain-days, as well as a decrease in the average intensity of rainfall (Figure 34). Over this region it appears that circulation changes (refer to the discussion in section 5.1) are inhibiting the formation of convective rainfall relative to the control simulations. Over the east coast of southern Africa, in the vicinity of southern Mozambique, the small changes in mean precipitation (Figure 28) are masking the increases in average rainfall intensity combined with decreases in rain-day frequency (Figure 34). For winter, the small reduction in mean rainfall over large regions of southern Africa is generally associated with reductions in both the number of rain-days and the rainfall intensity (Figure 34).

The summer mean dry period length (consecutive days with rainfall less than 0.2 mm) increases over parts of the west coast of southern Africa under the A2 scenario (Figure 35). This increase in dry spell length is thus coupled not only with a decrease in the number of rain-days (Figure 34), but also a reduction in the intensity of rainfall on those days when rainfall occurs (Figure 34). The change in mean wet period length (consecutive days with rainfall more than 0.2 mm) shows a broad region of central equatorial and tropical southern Africa where the mean wet period length decreases (Figure 35). The region north of about 10°S is, however, associated with increases in mean seasonal rainfall (Figure 28) and rainfall intensity (Figure 34), and is not associated with large increases in dry period length (Figure 35). This suggests that, firstly, over this region the mean seasonal rainfall increases because the rainfall intensity increases, and secondly, because there is not a large increase in the mean dry period length, it implies that there are more frequent dry periods interspersed between the wet spells thus causing the wet spell length to decrease. The same can be said for the increase in mean wet period length over central equatorial land regions in winter (Figure 35). Over much of tropical and subtropical southern Africa in winter there is an increase in the mean length (Figure 35) and frequency (because the mean wet period length does not change by a similar magnitude to the dry period length) of dry spells.

A GEV analysis has been performed on summer and winter daily precipitation from the control and A2 scenario simulations. Future changes in return values are interpreted in terms of changes in return periods for 1961-90 (i.e. control) GCM size events. In other words, return values for a 20-year return period are calculated from the control GCM results, as described in section 4.2 (Figure 17). Then, the return periods for the A2 scenario simulations which correspond to these control return values are calculated at each grid box. The results are shown in Figure 36. Values less (greater) than 20 imply that the control extreme precipitation event is more (less) likely in the future scenario. In summer much of equatorial Africa and eastern southern Africa display more extreme rainfall in the A2 scenario, with the one in 20-year event becoming of the order of a one in 5-year event in many regions. Over western tropical and subtropical southern Africa rainfall is less extreme. In winter, rainfall is more extreme in the A2 scenario over the winter rainfall region around the equator, and over eastern southern Africa south of 20°S, but less extreme over the rest of southern Africa. Results from a 50-year return period analysis (not shown) exhibit the same patterns of change.

The analysis of distributions of daily rainfall has been performed for the same South African regions as in section 4.2. In summer, east coast and eastern interior rainfall over South Africa is more extreme in the A2 scenario, whereas for the south western Cape, rainfall increases in the 20 – 30 mm/day class but decreases in most of the other classes (Figure 37). In winter over the east coast there are negligible changes; over the eastern interior there are reductions in rainfall in the 5-10 and 10-20 mm/day classes, but an increase in the 20-30 mm/day class; and over the south western Cape there is a reduction in rainfall in the most extreme rainfall classes (Figure 37).

6. SUMMARY

The present study has used a high resolution GCM, HadAM3H, to examine present-day and future possible climates over southern Africa. In order to gauge model performance, HadAM3H's simulation of the present-day (1961-90) climate has been compared to observed data, and the major findings are summarised below:

- The model captures the primary features of the observed circulation and the pattern of seasonal change is generally well represented for most variables.

- In summer, moisture convergence into the ITCZ and ZAB is too strong, resulting in a positive rainfall bias over much of southern Africa in the model.

- There is a surface temperature cold bias in the model over large regions of southern Africa, which is related to the likelihood of greater evaporative cooling in the model, as well as an excess of thick cloud, causing less incoming solar radiation to reach the earth's surface.

- In winter, surface temperatures south of 30°S are colder than observed, whereas between 10°S and 25°S there is a warm bias. These biases are related to cloud and circulation anomalies.

- The model performs relatively well in simulating the inter- and intra-annual variability of sea level pressure in summer and winter, as well as the interannual variability of seasonal mean precipitation.

- Over South Africa, the model tends to overestimate the number of rain-days and rainfall intensity in summer, particularly over central regions, whereas in winter the model reproduces the number of rain-days but underestimates rainfall intensity along the south and east coasts. Similar biases are found for extreme rainfall, such that the 20-year return values of daily

precipitation tend to be too large over central regions in summer and too small over coastal regions in winter.

HadAM3H has been run over the period 2071-2100 for both the A2 and B2 IPCC SRES emissions scenarios. Due to the stronger forcing in the A2 scenario, the scenario anomalies of surface temperature, precipitation and sea level pressure are generally larger than for the B2 scenario. The results over southern Africa for the A2 scenario suggest:

- a warming throughout the troposphere, with largest temperature increases over land areas. There is an average surface warming of 3.9°C in summer and 4.1°C in winter over southern Africa.

- that over western and central tropical and subtropical land areas in summer there are reductions in average rainfall, in the interannual variability of seasonal mean precipitation, in the number of rain-days and in the average intensity of rainfall. There is also a reduction in the probability of extreme rainfall events. It appears that circulation changes are inhibiting the formation of convective rainfall relative to the control simulations.

- that over equatorial regions in summer there is a general increase in average rainfall, an increase in the intensity of rainfall (rather than the number of rain-days) and an increased likelihood of extreme rainfall.

- that in winter in equatorial regions there is a general increase in seasonal mean rainfall and extreme rainfall events are more likely, but over the South Western Cape, winter rainfall region of South Africa, there is a reduction in mean seasonal rain and a tendency for extreme rainfall events to be less likely.

HadAM3H has been used to drive a regional climate model (resolution ~50km) over southern Africa for both the 30-year present-day and future periods in order to provide a more detailed analysis of climate change over the region, including the analysis of extreme events. These results are described by Hudson (2002) and Hudson and Jones (2002).

ACKNOWLEDGEMENTS

This study was carried out under the UK's Department for Environment, Food and Rural Affairs (DEFRA) Climate Prediction Programme (PECD 7/12/37), and the lead author was subcontracted to the Hadley Centre from the University of East Anglia (Climatic Research Unit) to perform the work. The Climate Systems Analysis Group (Department of Environmental and Geographical Science) at the University of Cape Town is thanked for access to the South African gridded precipitation data set. The lead author would also like to thank the University of Cape Town (Department of Environmental and Geographical Science) for granting her an extended period of special leave to pursue post-doctoral research in the United Kingdom.

REFERENCES

Gibson, R.K., Kallberg, P., Uppala, S., Hernandez, A., Nomura, A. and Serrano, E. 1997. ECMWF Re-Analysis Project Report Series, 1. ERA Description, ECMWF.

Gordon, C., Cooper, C., Senior, C., Banks, H., Gregory, J., Johns, T., Mitchell, J. and Wood, R. 2000. The simulation of SST, sea ice extents and ocean heat transports in a coupled model without flux adjustments. *Climate Dynamics*, 16: 147-168.

Harrison, E.F., Minnis, P., Barkstrom, B.R., Ramanathan, V. and Gibson, G.G. 1990. Seasonal variation of cloud radiative forcing derived from the Earth Radiation Budget Experiment. *Journal of Geophysical Research*, 95: 18687-18703.

Hewitson, B.C. and Crane, R.G. 1996. Climate downscaling: Techniques and application. *Climate Research***,** 7(2): 85-95.

Hobbs, J.E., Lindesay, J.A. and Bridgman, H.A. 1998. *Climates of the Southern Continents. Present, Past and Future*. Wiley and Sons, Chichester.

Hosking, J.R.M. 1990. L-moments: Analysis and estimation of distributions using linear combinations of order statistics. *Journal of the Royal Statistical Society*, 52B: 105-124.

Hudson, D.A. 2002. Future changes in temperature and precipitation extremes over southern Africa. DEFRA Report 2/2/02, Hadley Centre for Climate Prediction and Research, Met Office, Bracknell, U.K.

Hudson, D.A. and Jones, R.G. 2002. Simulating present-day and future climates of southern Africa using the Hadley Centre regional climate model. Hadley Centre Technical Note (in preparation), Hadley Centre for Climate Prediction and Research, Met Office, Bracknell, U.K.

Intergovernmental Panel on Climate Change (IPCC), 2000. Special Report on Emissions Scenarios. Nakicenovic, N. and Swart, R. (eds.). Cambridge University Press, UK. pp 570

Intergovernmental Panel on Climate Change (IPCC), 2001. *Climate Change 2001 - The Scientific Basis: Contribution of Working Group 1 to the Third Assessment Report of the Intergovernmental Panel on Climate Change.* J.T. Houghton, Y. Ding, D.J. Griggs, M. Noguer, P.J. van der Linden, X. Dai, K. Maskell, C.A. Johnson (eds.), Cambridge University Press, Cambridge, United Kingdom and New York, NY, USA, 881pp.

Johns, T.C., Gregory, J.M., Ingram, W.J., Johnson, C.E., Jones, A., Lowe, J.A., Mitchell, J.F.B., Roberts, D.L., Sexton, D.M.H., Stevenson, D.S., Tett, S.F.B. and Woodage, M.J. 2001. Anthropogenic climate change for 1860 to 2100 simulated with the HadCM3 model under updated emissions scenarios. Hadley Centre Technical Note No. 22, Hadley Centre for Climate Prediction and Research, Met Office, Bracknell, U.K.

Jones, R., Hassell, D. and Murphy, J. 1999. Configuring new climate models for Europe with improved climatologies via better representation of physical processes. UKMO second year report for MERCURE, EC contract ENV4-CT97-0485.

Kharin, V.V. and Zwiers, F.W. 2000. Changes in the extremes in an ensemble of transient climate simulations with a coupled atmosphere-ocean GCM. *Journal of Climate*, 13:3760-3788.

New, M., Hulme M. and Jones, P. 1999. Representing twentieth-century space-time climate variability. Part I: Development of a 1961-90 mean monthly terrestrial climatology. *Journal of Climate*, 12: 829-856.

Murphy, J.M., Jones, R.G., Hassell, D.C. and Woodage, M.J. 2002. A high resolution atmospheric GCM for the generation of regional climate scenarios. (In preparation).

Nicholson, S.E., Kim, J. and Hoopingarner, J. 1988. *Atlas of African Rainfall and its Interannual Variability*. Department of Meteorology, The Florida State University, Tallahasse, 237pp.

Pope, V.D., Gallani, M.L., Rowntree, P.R. and Stratton, R.A. 2000. The impact of new physical parametrizations in the Hadley Centre climate model: HadAM3. *Climate Dynamics*, 16: 123-146.

Rayner, N.A., Parker, D.E., Horton, E.B., Folland, C.K., Alexander, L.V., Rowell, D.P., Kent, E.C. and Kaplan, A. 2002. Global analyses of SST, sea ice and night marine air temperature since the late nineteenth century. Submitted to Journal of Geographical Research (Atmospheres).

Rossow, W.B. and Schiffer, R.A. 1991. ISCCP cloud data products. *Bulletin of the American Meteorological Society*, 72: 2-20

Simmons, A.J. and Burridge, D.M. 1981. An energy and angular-momentum conserving finite-difference scheme and hybrid coordinates. *Monthly Weather Review*, 109:758-766.

Stratton, R.A. 1999. A high resolution AMIP integration using the Hadley Centre model HadAM2b. *Climate Dynamics*, 15:9-28.

Tyson, P.D. and Preston-Whyte, R.A. 2000. *The Weather and Climate of Southern Africa*. Oxford University Press, Cape Town.

Von Storch, H., Zorita, E. and Cubasch, U. 1993. Downscaling of global climate Change estimates to regional scales: An application to Iberian rainfall in wintertime. *Journal of Climate*, 6: 1161-1171.

Xie, P. and Arkin, P.A. 1997. Global precipitation: a 17-year monthly analysis based on gauge observations, satellite estimates and numerical model outputs. *Bulletin of the American Meteorological Society*, 78: 2539-2558.

DJF: 1.5 m Temperature (°C)				
	Mean	Spatial Std dev.	Spatial Min	Spatial Max
CONTROLS	22.64	2.29	16.10	29.19
	22.62	2.22	16.09	28.99
	22.69	2.27	16.15	29.18
FUTURE A2	26.45	2.41	19.80	32.27
	26.69	2.50	20.12	32.71
	26.57	2.43	20.05	31.76
FUTURE B2	25.33	2.34	18.86	30.62
JJA: 1.5 m Temperature (°C)				
CONTROLS	19.59	4.29	6.48	27.59
	19.55	4.25	6.46	27.58
	19.59	4.23	6.58	27.53
FUTURE A2	23.67	4.58	10.62	30.90
	23.63	4.69	10.63	31.18
	23.67	4.67	10.68	31.26
FUTURE B2	22.38	4.53	9.11	29.69

Table 1: 1.5 m temperature (°C) results taken from the 30-year seasonal mean field over southern Africa (land points only) for the three control and A2 scenario simulations respectively, and the single B2 simulation, in summer (DJF) and winter (JJA). The standard deviation, minimum and maximum values thus represent spatial variation over the seasonal mean field.

DJF: Precipitation (mm/day)				
	Mean	Spatial Std dev.	Spatial Min	Spatial Max
CONTROLS	5.29	2.44	0.19	14.32
	5.39	2.54	0.18	15.71
	5.33	2.46	0.23	14.38
FUTURE A2	5.22	2.54	0.10	16.23
	4.85	2.36	0.14	12.73
	5.15	2.55	0.14	15.74
FUTURE B2	5.19	2.43	0.16	13.29
JJA: Precipitation (mm/day)				
CONTROLS	0.47	0.87	0.00	5.14
	0.49	0.90	0.00	5.21
	0.47	0.88	0.00	5.07
FUTURE A2	0.39	0.81	0.00	5.46
	0.36	0.77	0.00	5.28
	0.37	0.80	0.00	5.44
FUTURE B2	0.41	0.83	0.00	5.32

Table 2: As for Table 1, but for precipitation (mm/day).

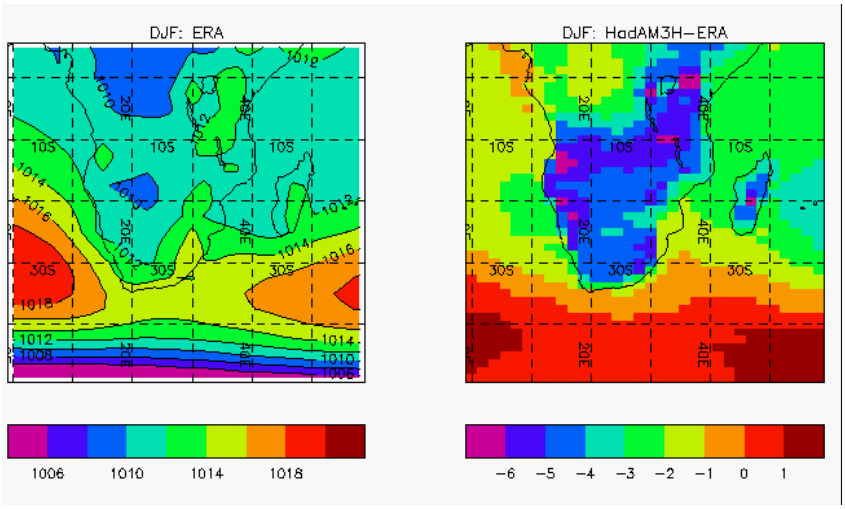

Figure 1: Sea level pressure (hPa) from the ERA reanalysis data (1979-1993) (Gibson *et al.*, 1997) and HadAM3H errors relative to this climatology for December to February (DJF).

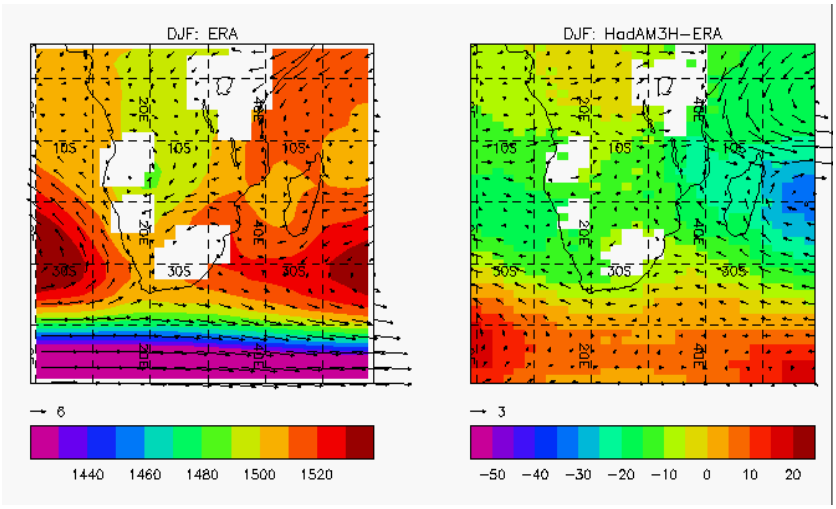

Figure 2: 850 hPa geopotential height contours (m) and wind vectors (m/s) from the ERA reanalysis data (1979-1993) (Gibson *et al.*, 1997) and HadAM3H errors relative to this climatology for December to February (DJF).

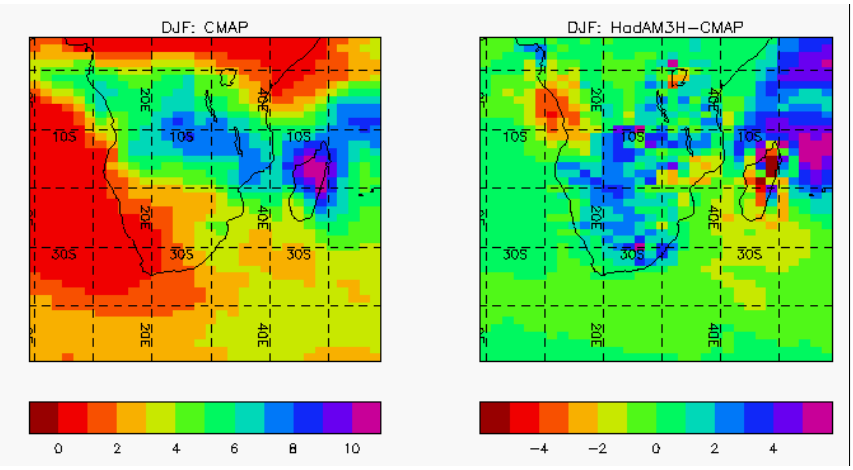

Figure 3: Precipitation (mm/day) from the CMAP data (1979-1999) (Xie and Arkin, 1997) and HadAM3H errors relative to this climatology for December to February (DJF).

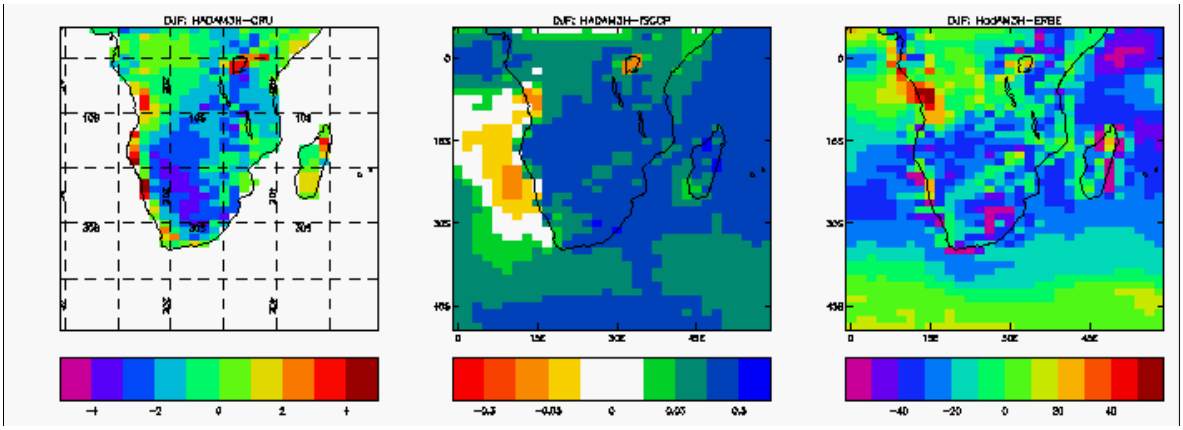

Figure 4: 1.5 m temperature (°C) (left), thick cloud fraction (middle) and shortwave cloud forcing (W/m^2) (right) errors in HadAM3H relative to the CRU climatology (1961-1990) (New *et al*., 1999), ISCCP data (1989-1993) (Rossow and Shiffer, 1991) and ERBE data (1985-1990) (Harrison *et al*., 1990) respectively for December to February (DJF).

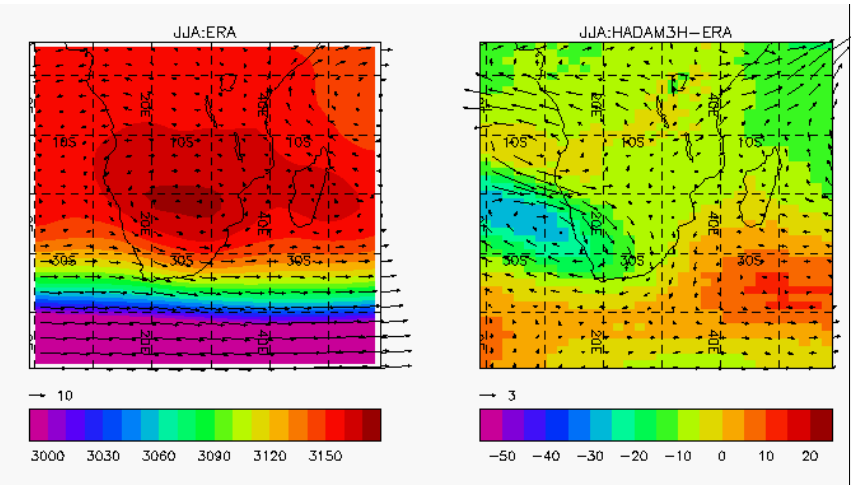

Figure 5: 700 hPa geopotential height contours (m) and wind vectors (m/s) from the ERA reanalysis data (1979-1993) (Gibson *et al*., 1997) and HadAM3H errors relative to this climatology for June to August (JJA).

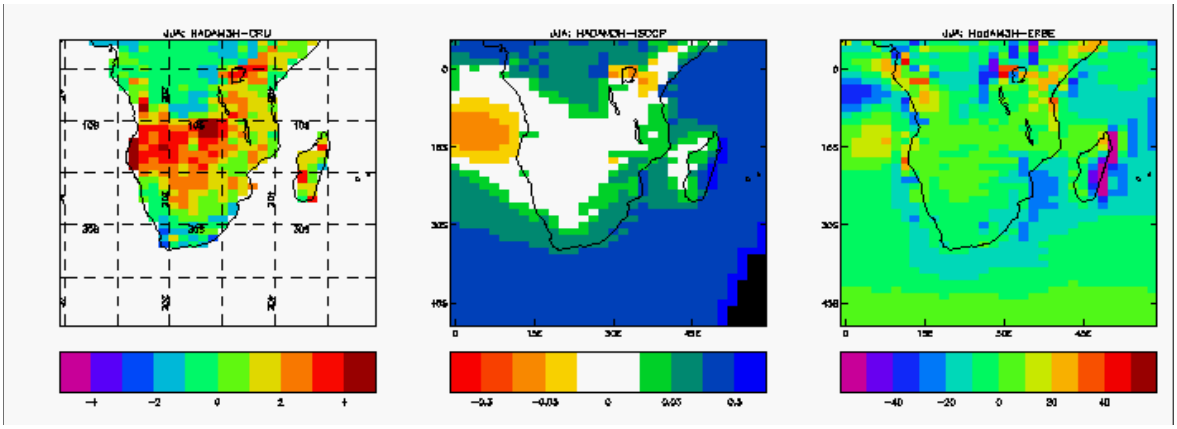

Figure 6: 1.5 m temperature (°C) (left), thick cloud fraction (middle) and shortwave cloud forcing (W/m^2) (right) errors in HadAM3H relative to the CRU climatology (1961-1990) (New *et al*., 1999), ISCCP data (1989-1993) (Rossow and Shiffer, 1991) and ERBE data (1985-1990) (Harrison *et al*., 1990) respectively for June to August (JJA).

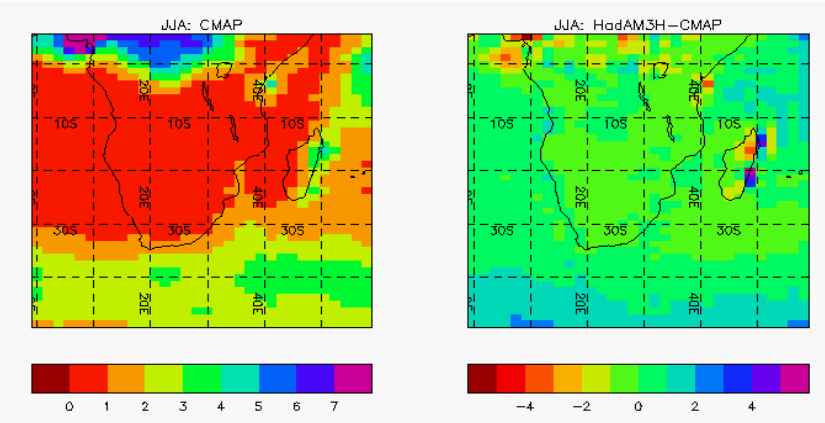

Figure 7: Precipitation (mm/day) from the CMAP data (1979-1999) (Xie and Arkin., 1997) and HadAM3H errors relative to this climatology for June to August (JJA).

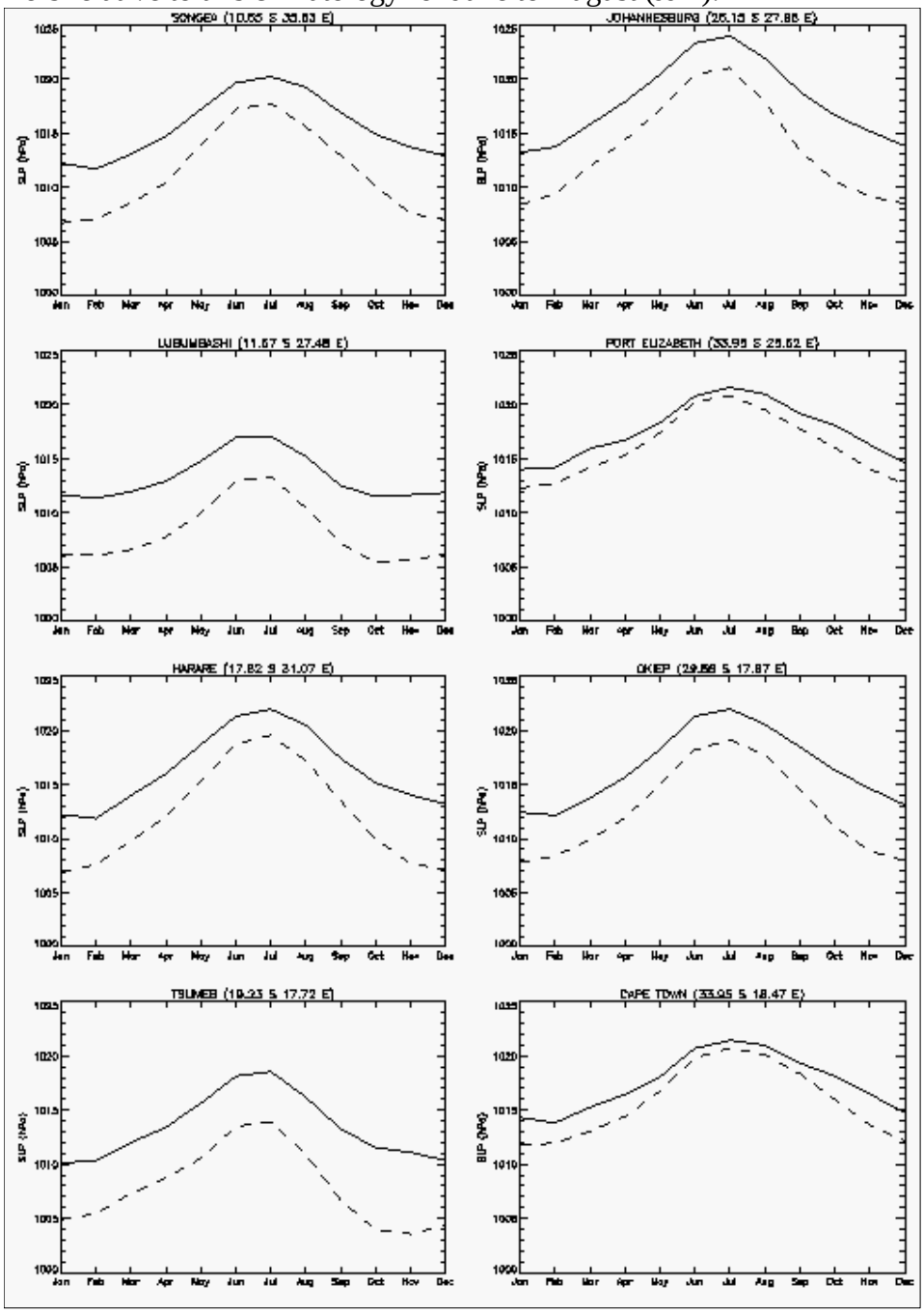

Figure 8: Seasonal cycle of sea level pressure (hPa) for the ERA reanalysis data (1979-1993) (Gibson *et al*., 1997) (solid line) and HadAM3H (dashed line) for select African stations.

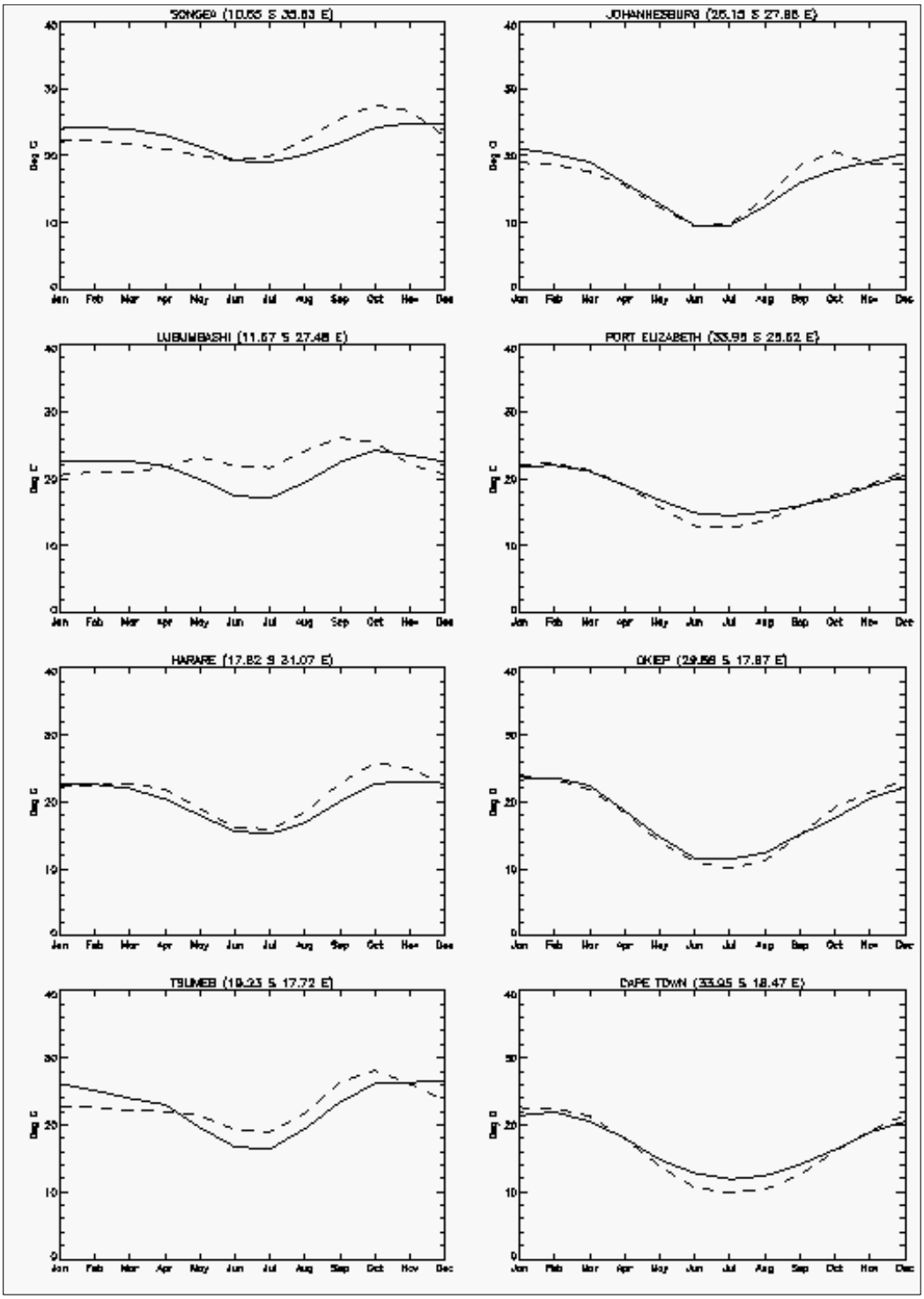

Figure 9: Seasonal cycle of 1.5 m temperature (°C) for the CRU climatology (1961-1990) (New *et al*., 1999) (solid line) and HadAM3H (dashed line) for select African stations.

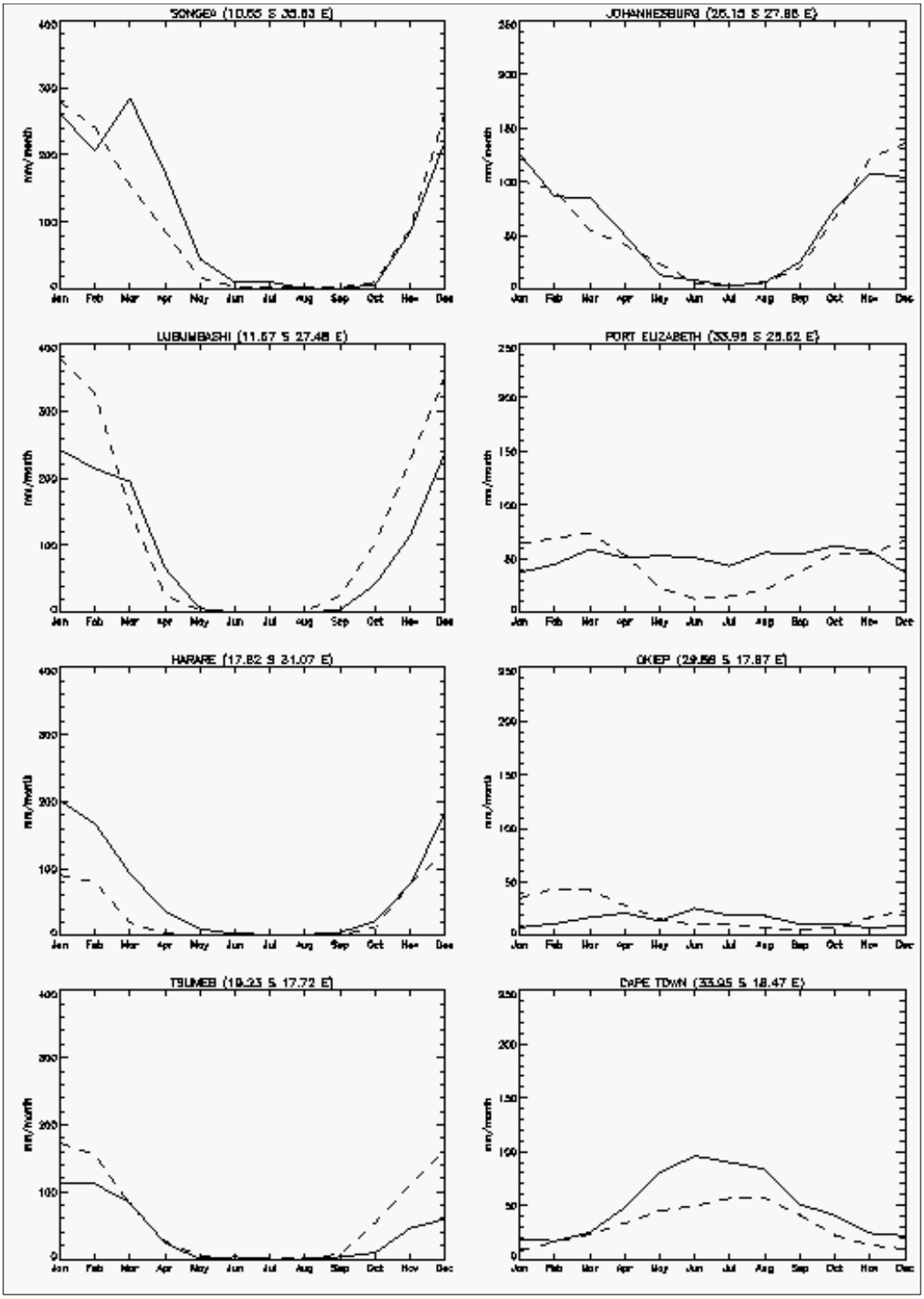

Figure 10: Seasonal cycle of precipitation (mm/month) for the CRU climatology (1961-1990) (New *et al*., 1999) (solid line) and HadAM3H (dashed line) for select African stations.

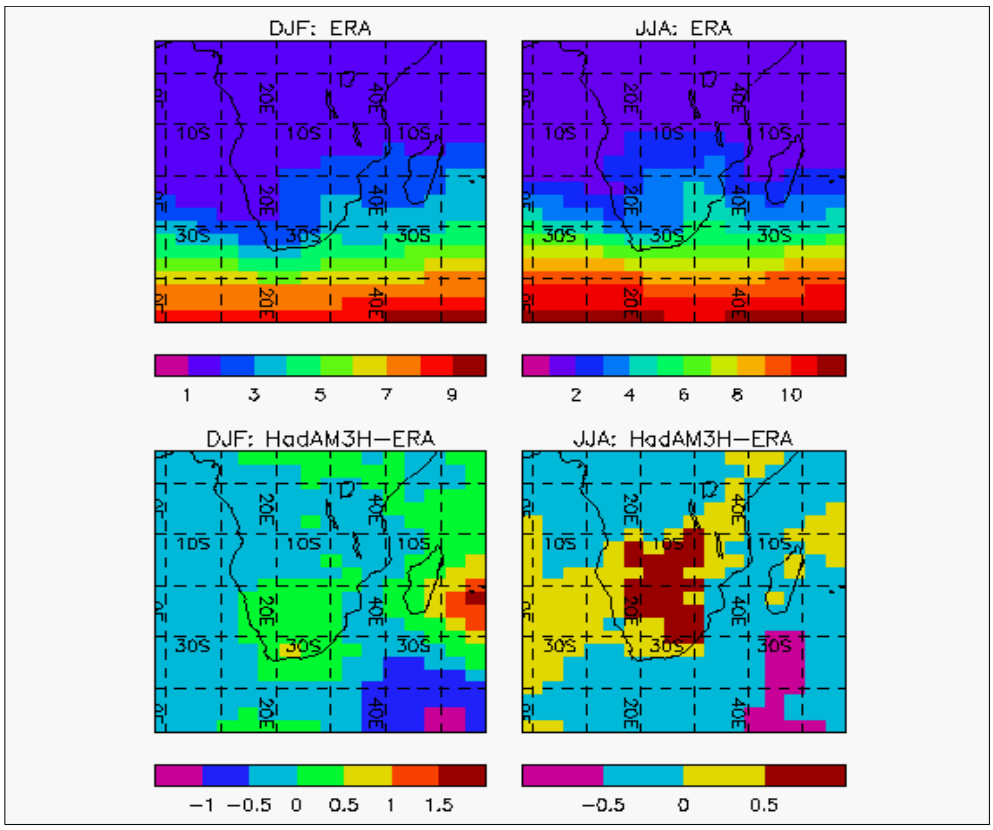

Figure 11: Intraseasonal variability of sea level pressure (hPa) (standard deviation of daily values from the respective seasonal mean) for the ERA reanalysis data (1979-1993) (Gibson *et al.*, 1997), and HadAM3H errors relative to this climatology for both December to February (DJF) and June to August (JJA).

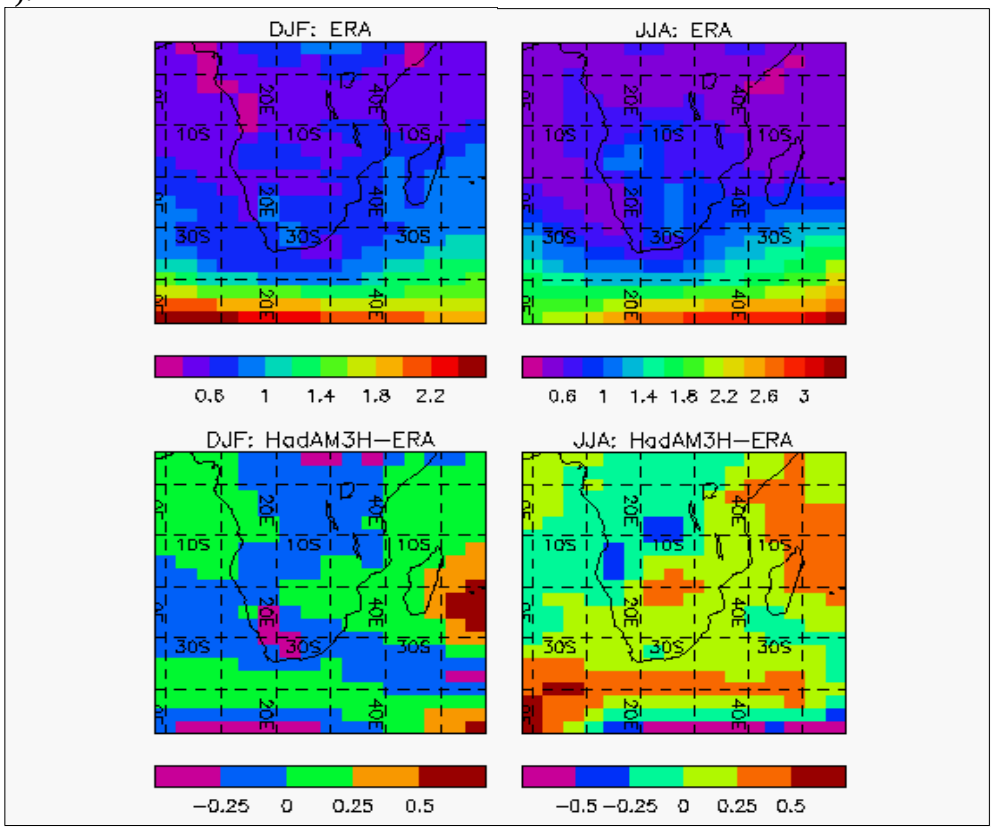

Figure 12: Interannual variability of the seasonal mean sea level pressure (hPa) for the ERA reanalysis data (1979-1993) (Gibson *et al.*, 1997), and HadAM3H errors relative to this climatology for both December to February (DJF) and June to August (JJA).

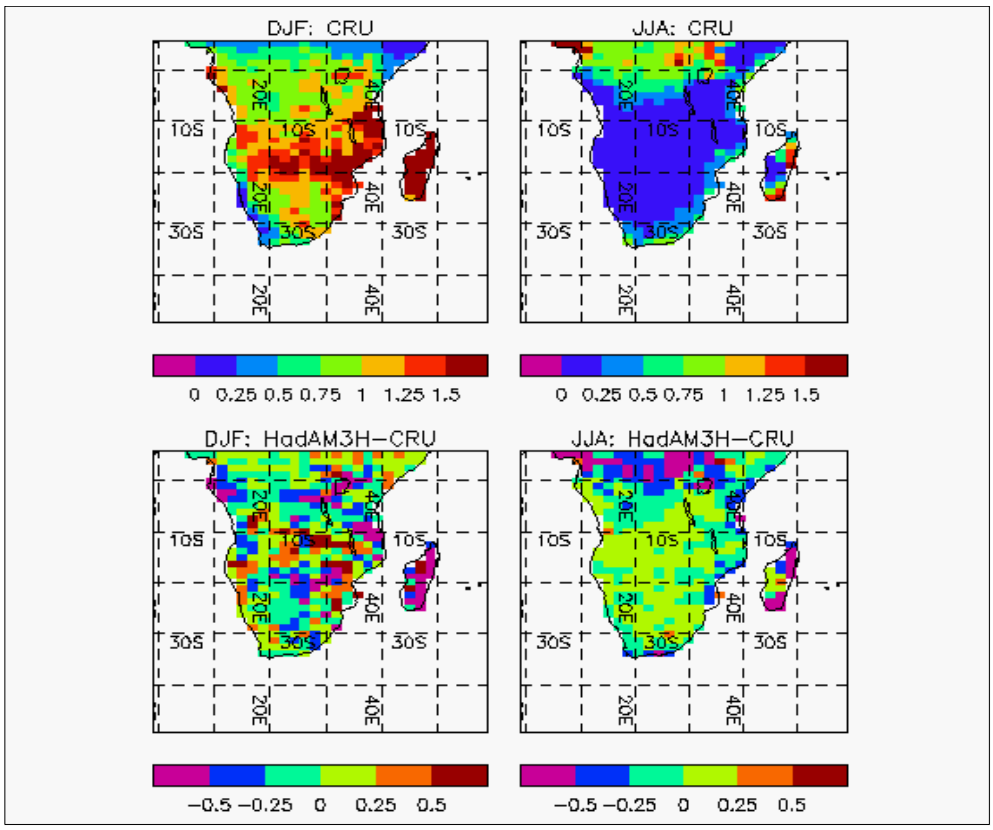

Figure 13: Interannual variability of seasonal mean precipitation (mm/day) for the CRU climatology (1961-1990) (New *et al.*, 1999), and HadAM3H errors relative to this climatology for both December to February (DJF) and June to August (JJA).

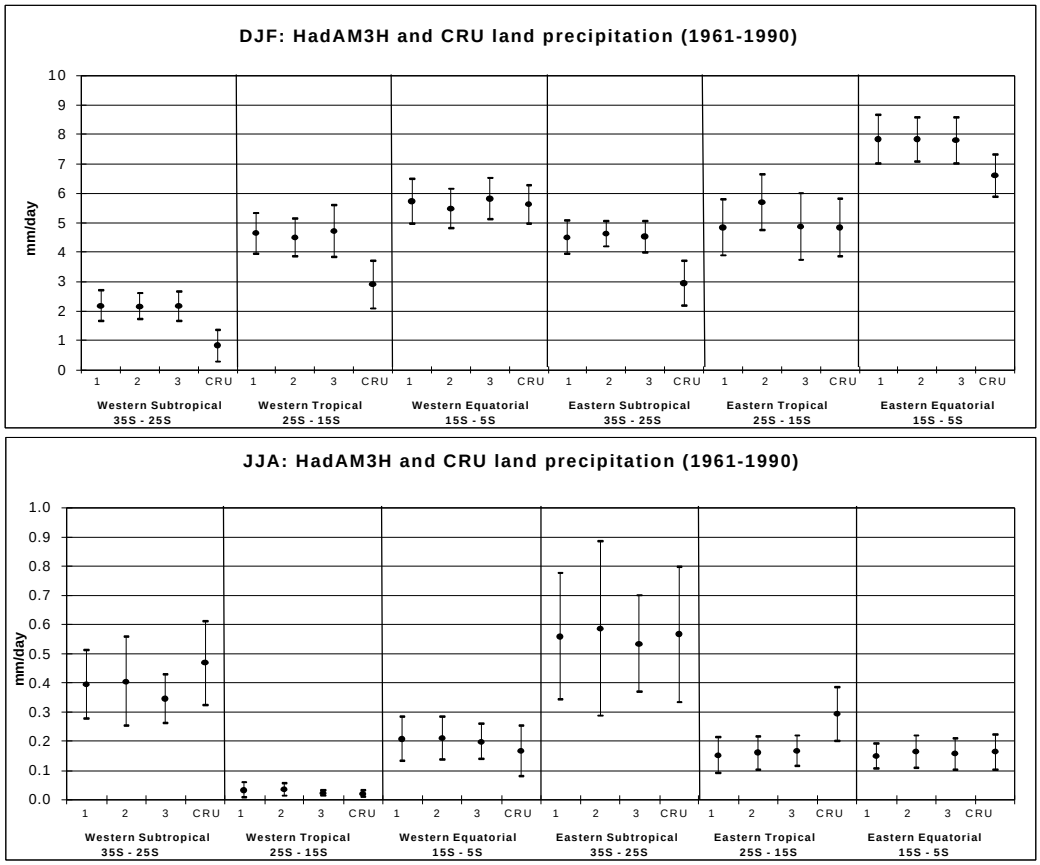

Figure 14: The mean and standard deviations of area-averaged seasonal mean land precipitation (mm/day) for the CRU climatology (1961-1990) (New *et al.*, 1999), and the three HadAM3H replicate simulations for December to February (DJF) and June to August (JJA). Southern Africa is split into 6 regions with 24°E as the dividing meridian.

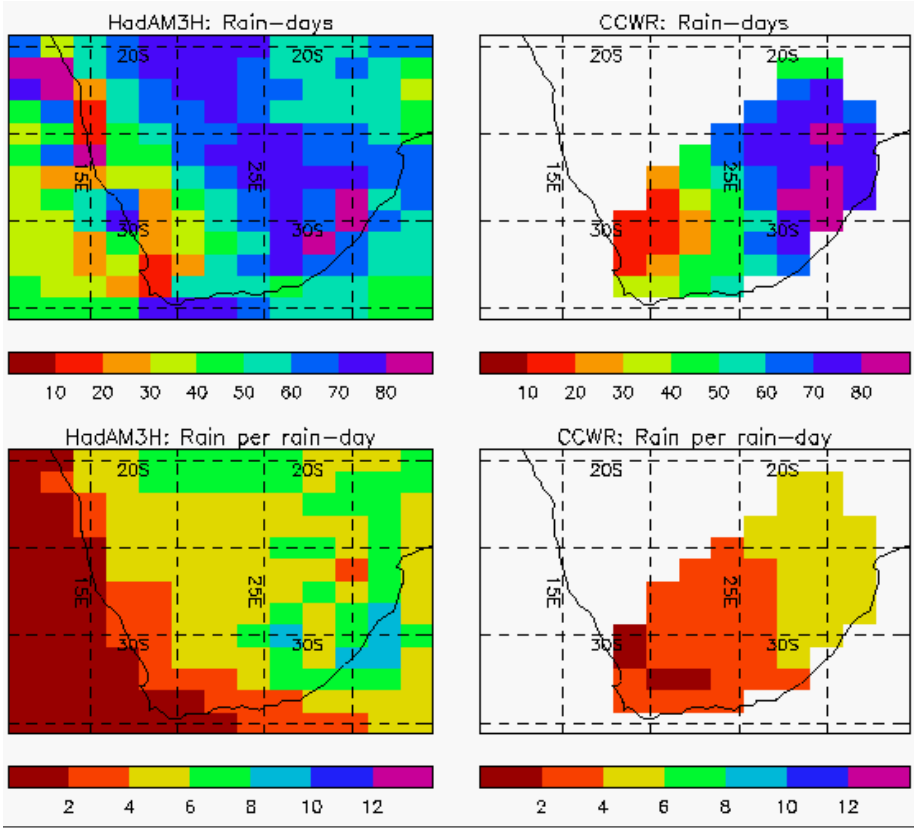

Figure 15: The average number of rain-days and rain per rain-day (mm) from HadAM3H (1961-1990) and the CCWR data (1950-1997) for December to February (DJF).

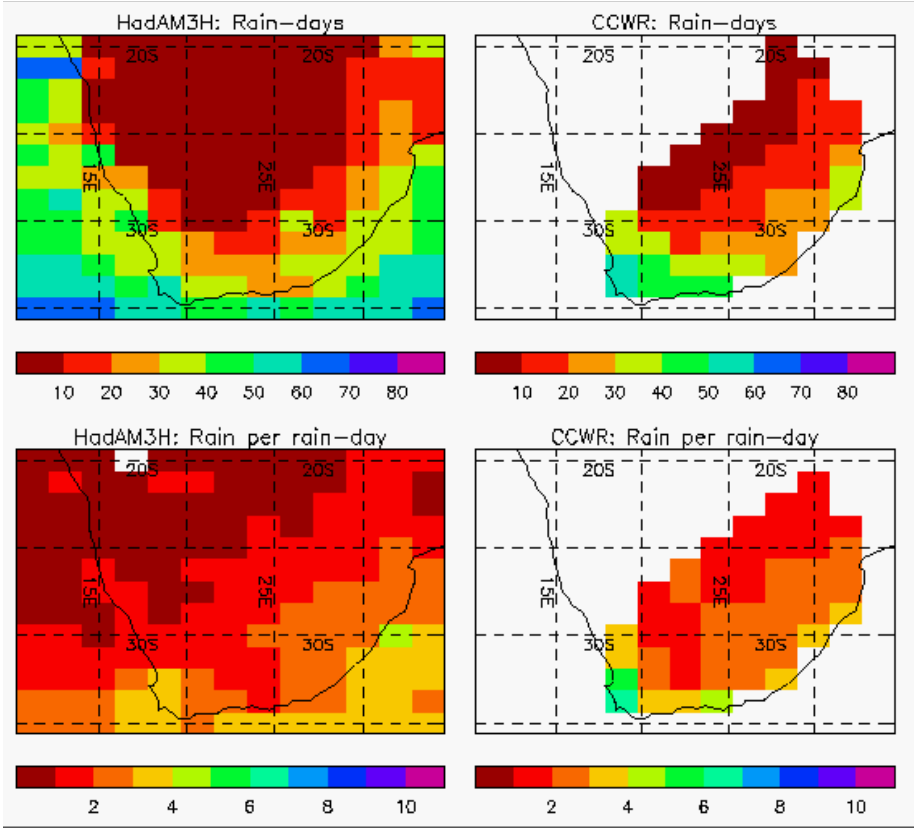

Figure 16: The average number of rain-days and rain per rain-day (mm) from HadAM3H (1961-1990) and the CCWR data (1950-1997) for June to August (JJA).

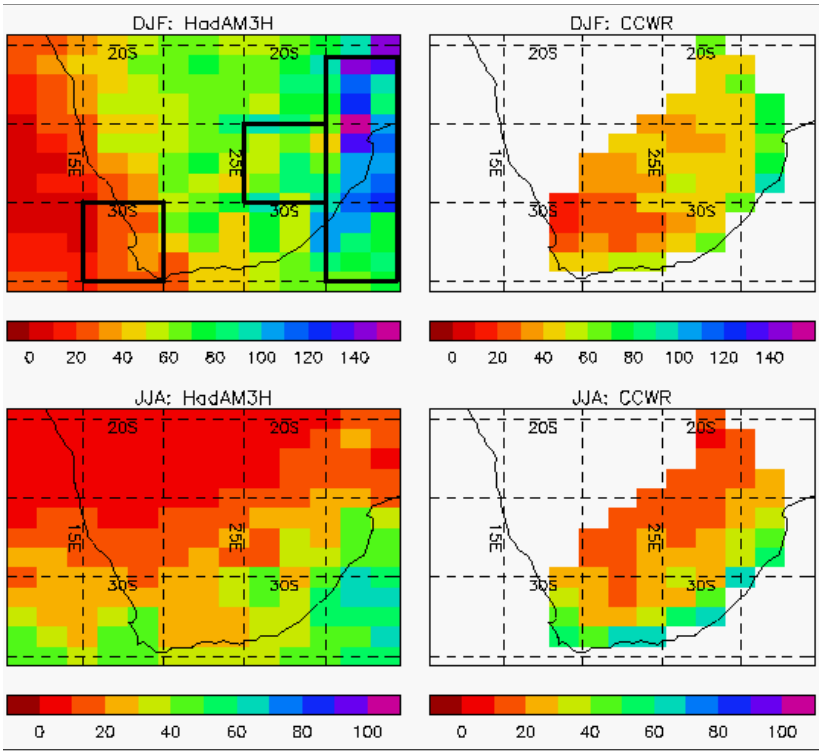

Figure 17: 20-year return values (mm/day) of daily precipitation from HadAM3H (1961-1990) and the CCWR data (1950-1997) for December to February (DJF) and June to August (JJA). The 3 boxes marked on the top left map refer to regions used for Figure 18.

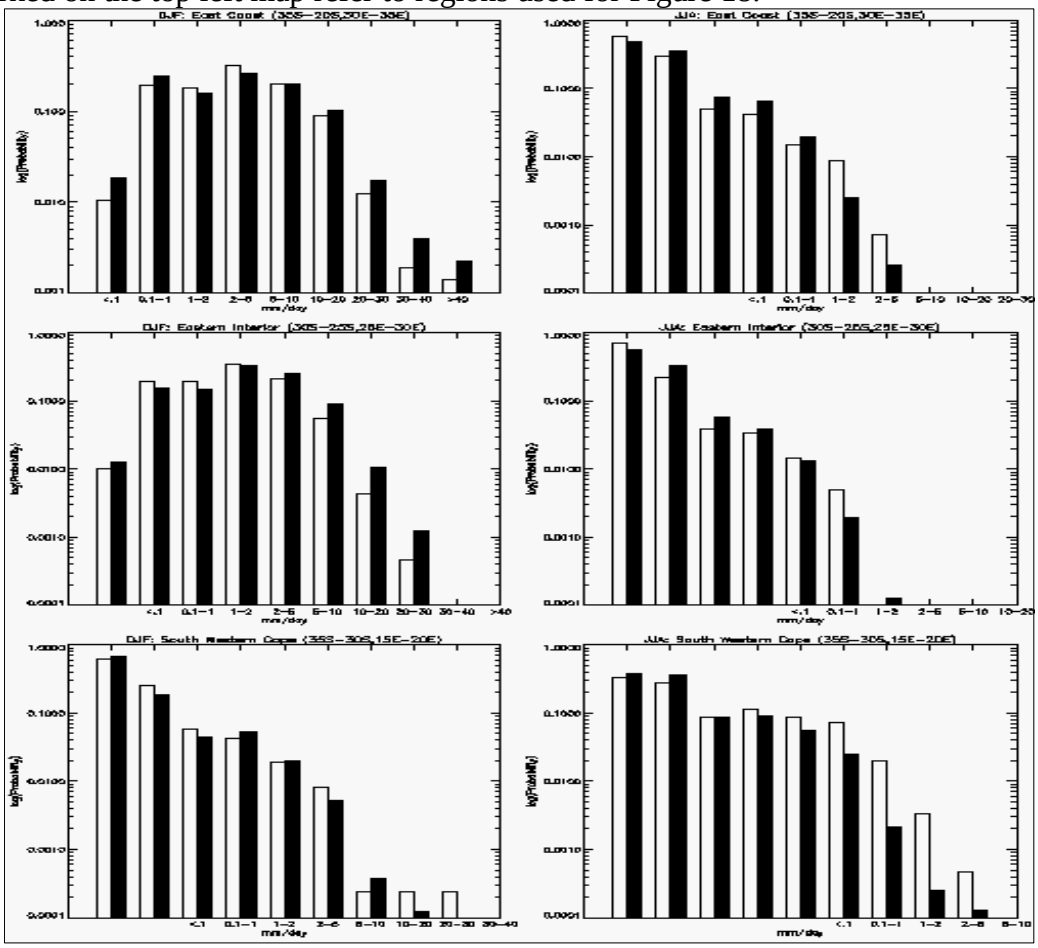

Figure 18: Histograms of the estimated probability (log scale) of rainfall (mm/day) falling in different classes for three land regions of South Africa (marked on Figure 17) from the CCWR observed data (1950-1997) (open bars) and HadAM3H data (solid bars) for December to February (DJF) and June to August (JJA).

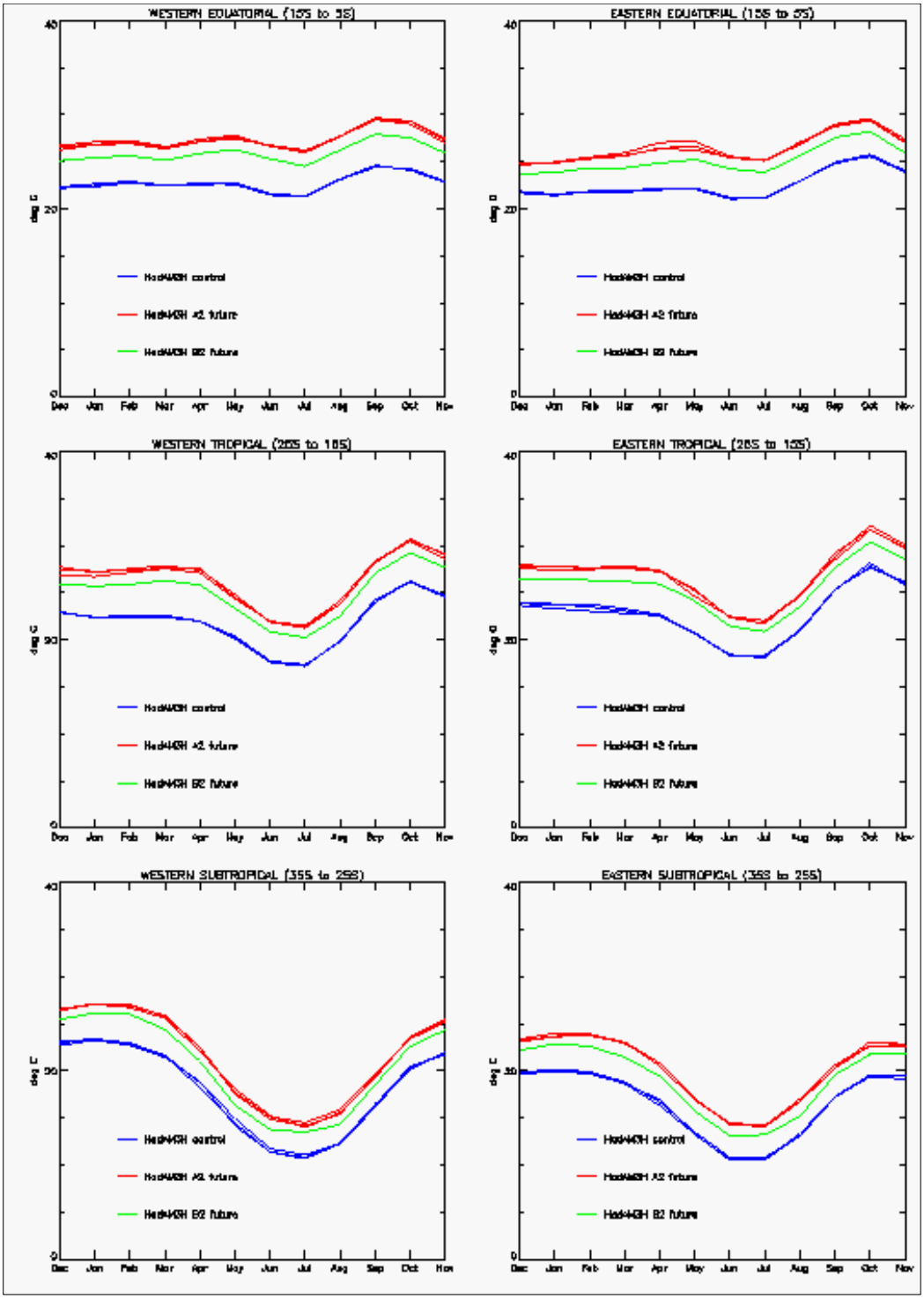

Figure 19: Seasonal cycle of the 30-year mean 1.5 m temperature (°C) for the control and SRES A2 and B2 scenario simulations, area averaged over 6 land regions of southern Africa with 24°E as the diving meridian.

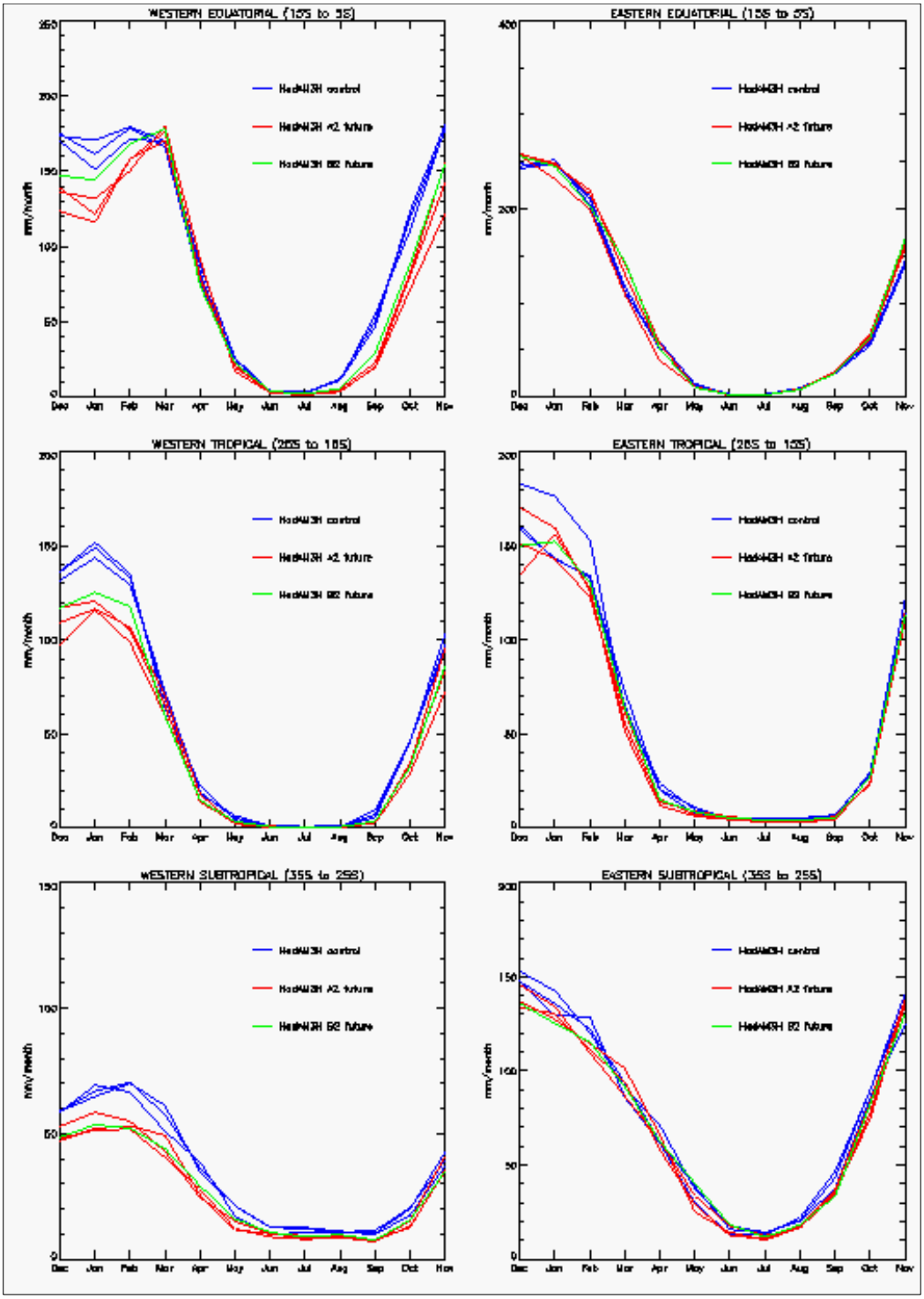

Figure 20: Seasonal cycle of the 30-year mean precipitation (mm/month) for the control and SRES A2 and B2 scenario simulations, area averaged over 6 land regions of southern Africa with 24°E as the diving meridian.

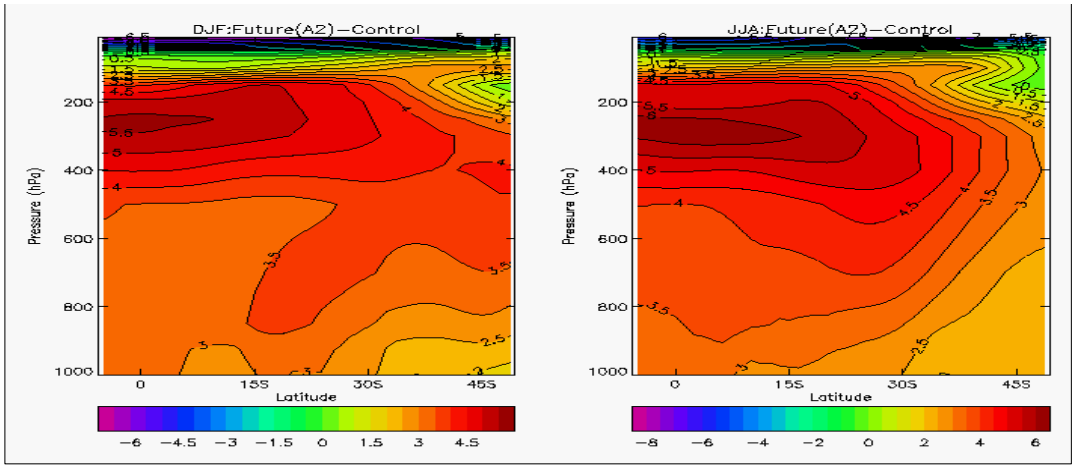

Figure 21: Vertical cross-section of the zonally averaged (between 0° and 59.28°E) temperature (°C) difference between the SRES A2 scenario and control simulations for December to February (DJF) and June to August (JJA).

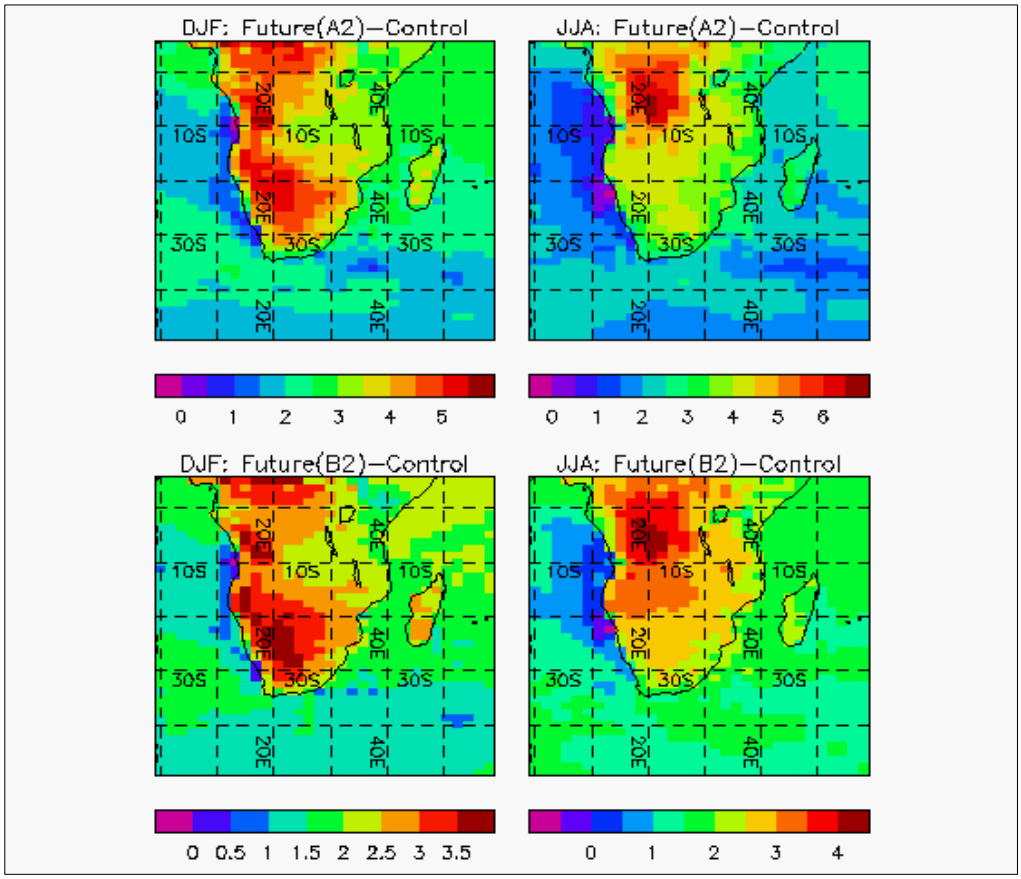

Figure 22: Thirty-year mean difference between the 1.5 m temperature (°C) simulated by the A2 and B2 SRES scenarios respectively and control simulations for December to February (DJF) and June to August (JJA).

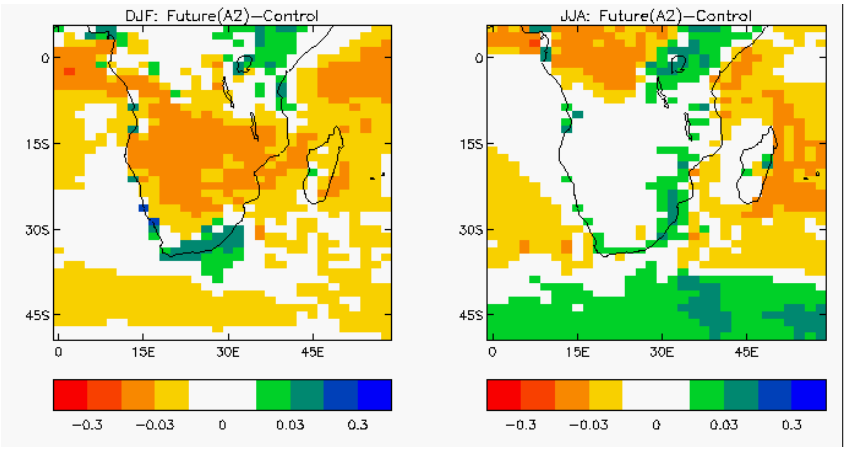

Figure 23: Thirty-year mean difference between the thick cloud fraction simulated by the SRES A2 scenario and control simulations for December to February (DJF) and June to August (JJA).

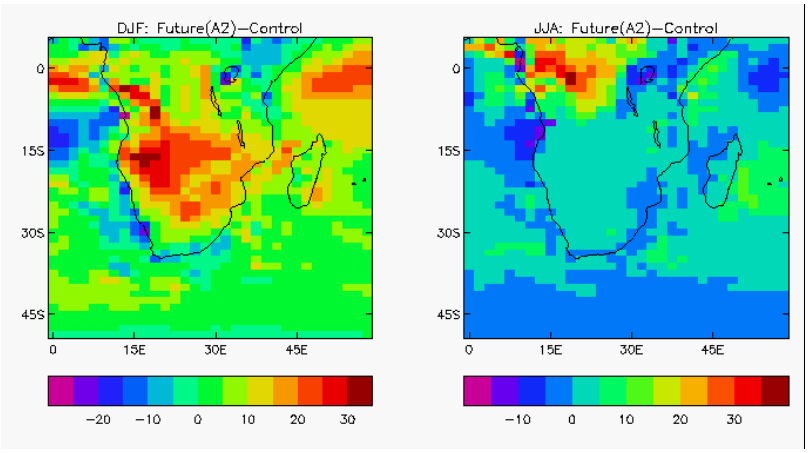

Figure 24: Thirty-year mean difference between the shortwave cloud forcing (W/m^2) simulated by the SRES A2 scenario and control simulations for December to February (DJF) and June to August (JJA). Negative values indicate increased shortwave cloud forcing (i.e. increased outgoing shortwave radiation).

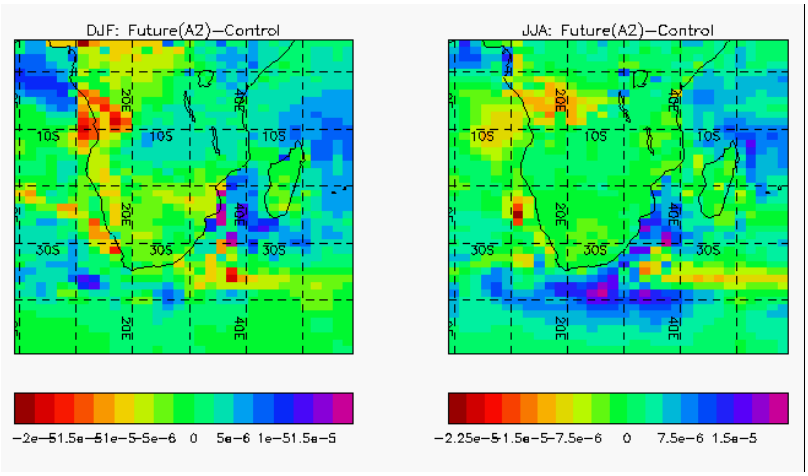

Figure 25: Thirty-year mean difference between the surface total moisture flux ($kg/m^2/s$) simulated by the SRES A2 scenario and control simulations for December to February (DJF) and June to August (JJA).

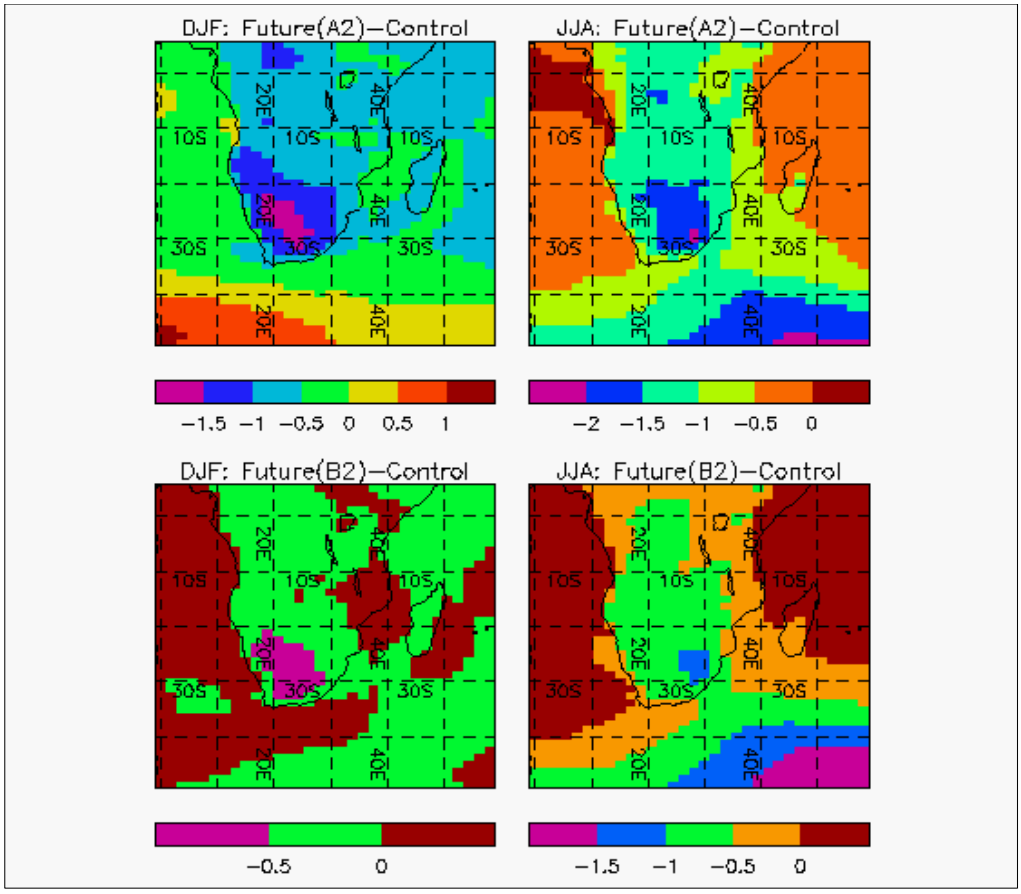

Figure 26: Thirty-year mean difference between the sea level pressure (hPa) simulated by the A2 and B2 SRES scenarios respectively and control simulations for December to February (DJF) and June to August (JJA).

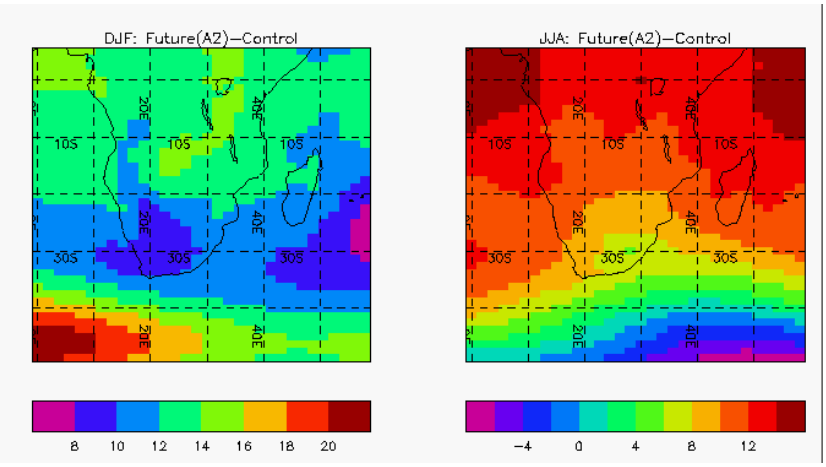

Figure 27: Thirty-year mean difference between the 850 hPa geopotential heights (m) simulated by the SRES A2 scenario and control simulations for December to February (DJF) and June to August (JJA).

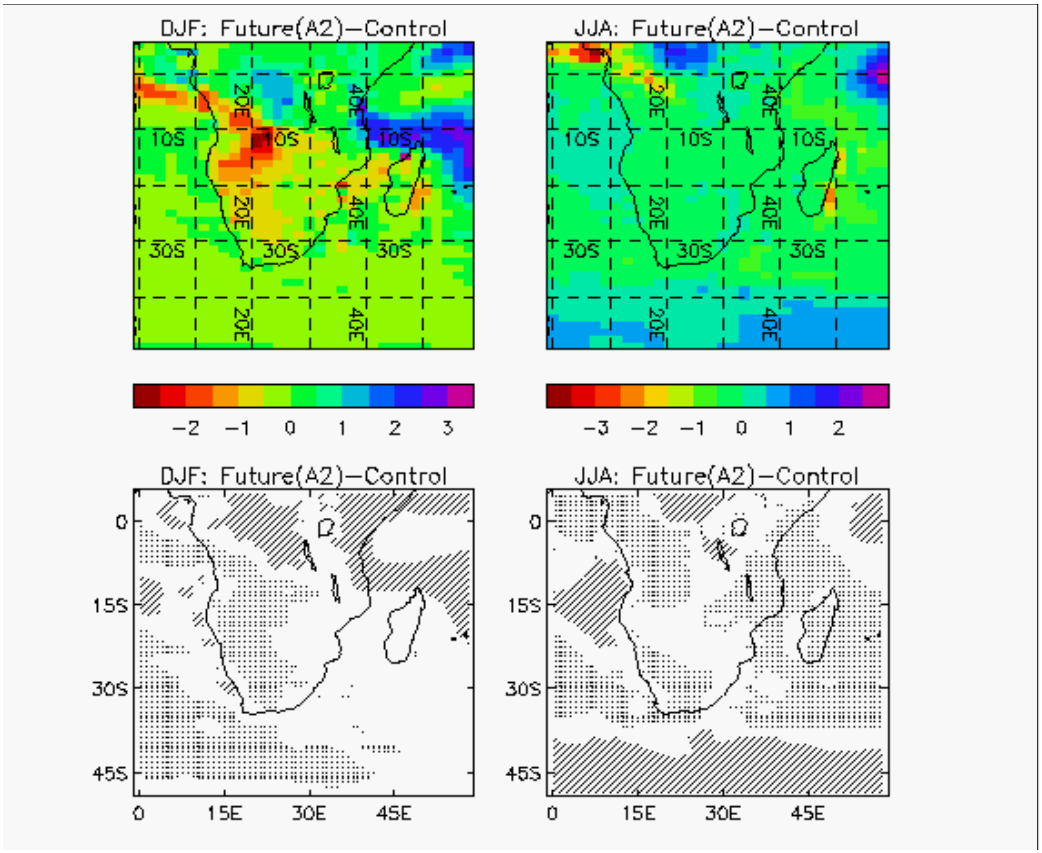

Figure 28: Thirty-year mean difference between the total precipitation (mm/day) simulated by the SRES A2 scenario and control simulations for December to February (DJF) and June to August (JJA). The lower diagrams show the statistically significant increases (lines) and decreases (stippled) at the 1% significance level (Students-T test).

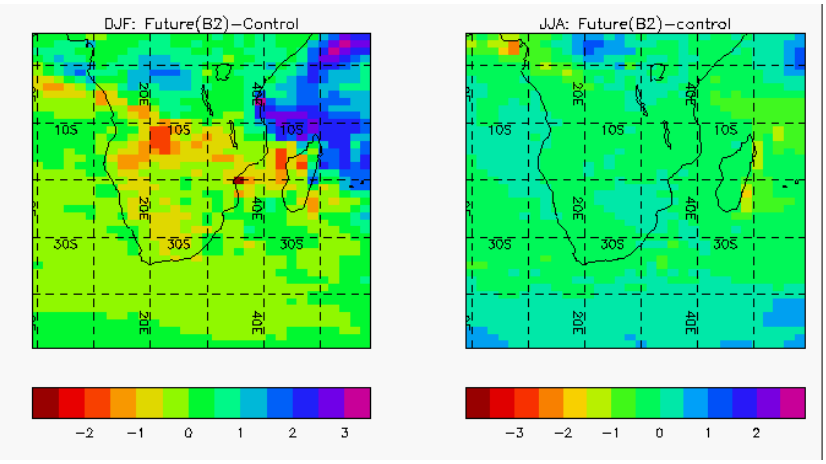

Figure 29: Thirty-year mean difference between the total precipitation (mm/day) simulated by the SRES B2 scenario simulation and the control simulations for December to February (DJF) and June to August (JJA).

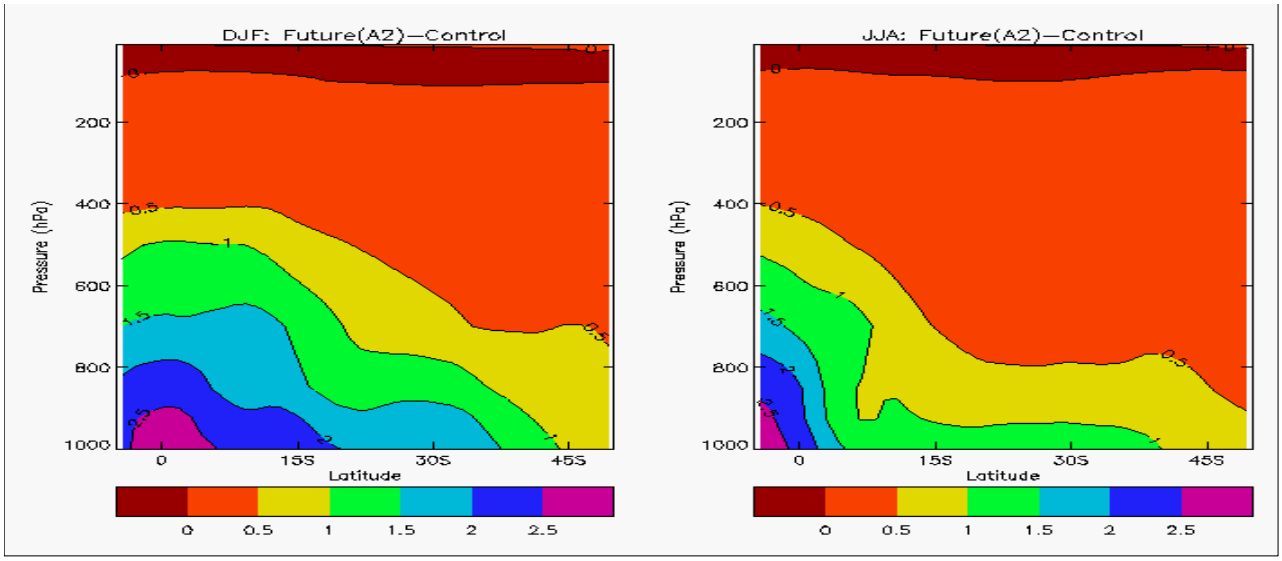

Figure 30: Vertical cross-section of the zonally averaged (between 0° and 59.28°E) specific humidity (g/kg) difference between the SRES A2 scenario and control simulations for December to February (DJF) and June to August (JJA).

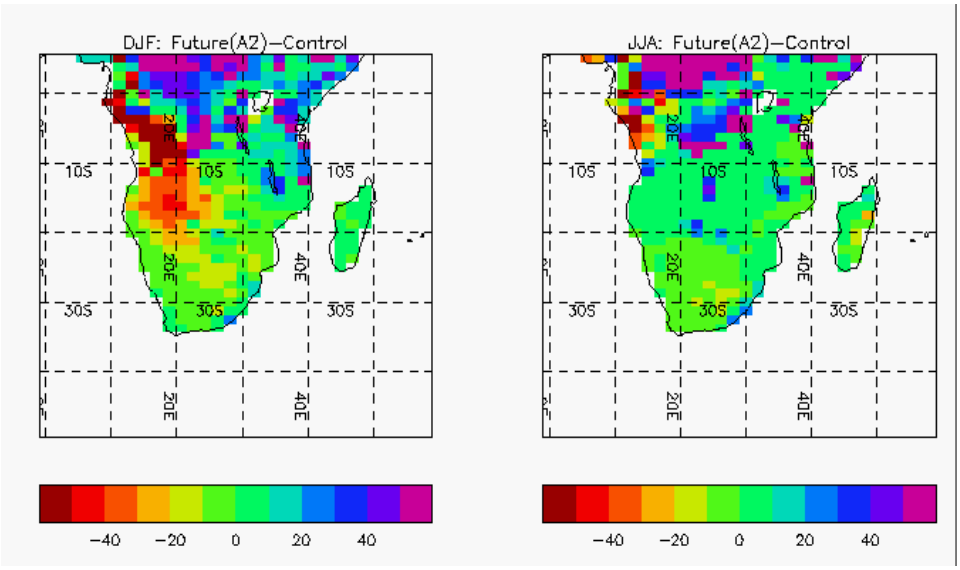

Figure 31: Thirty-year mean difference between the soil moisture content (cm) simulated by the SRES A2 scenario and control simulations for December to February (DJF) and June to August (JJA).

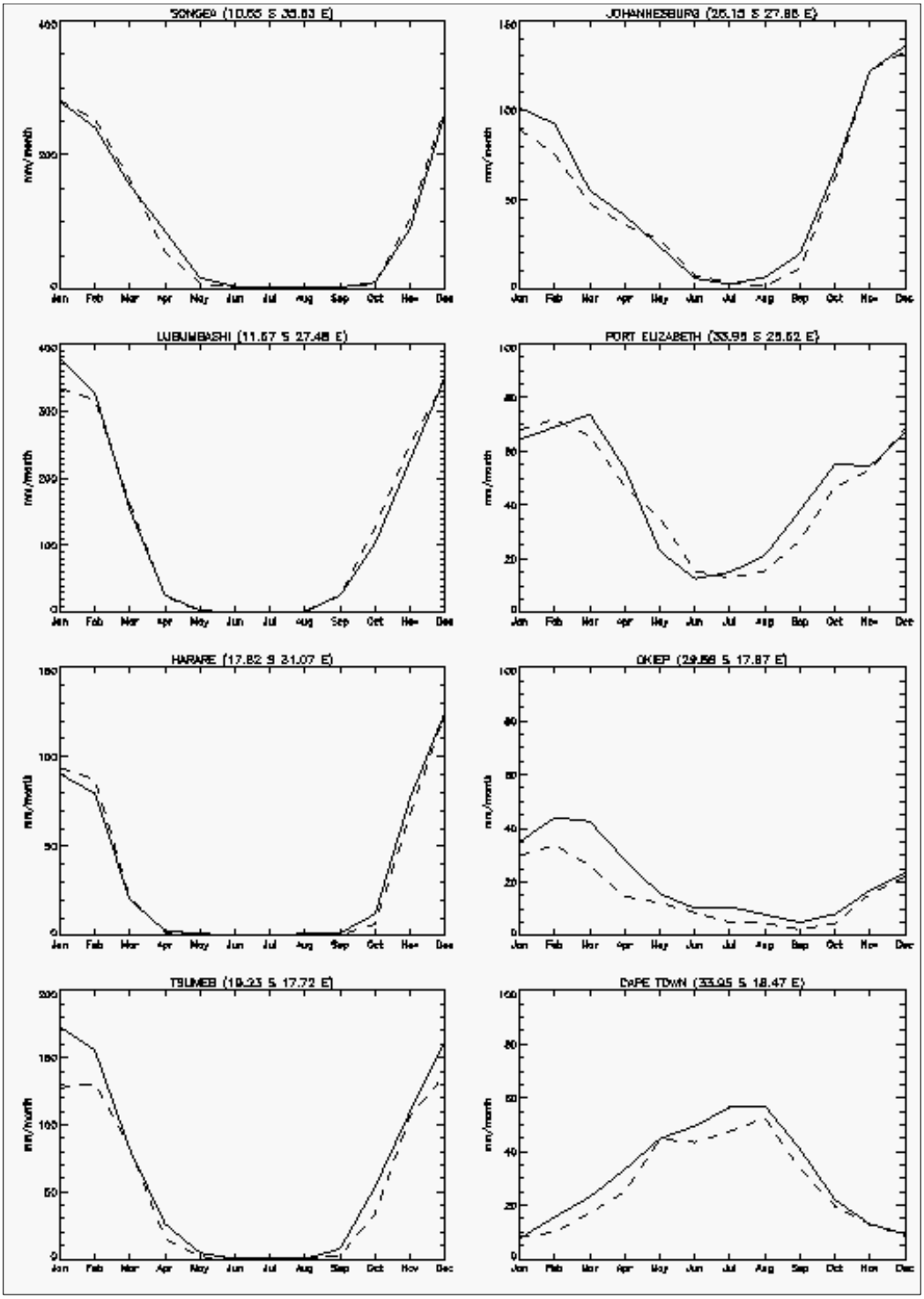

Figure 32: Seasonal cycle of the 30-year mean precipitation (mm/month) for the control (solid line) and SRES A2 scenario (dashed line) simulations for select African stations. (Note: only one simulation from the A2 ensemble has been used for this analysis).

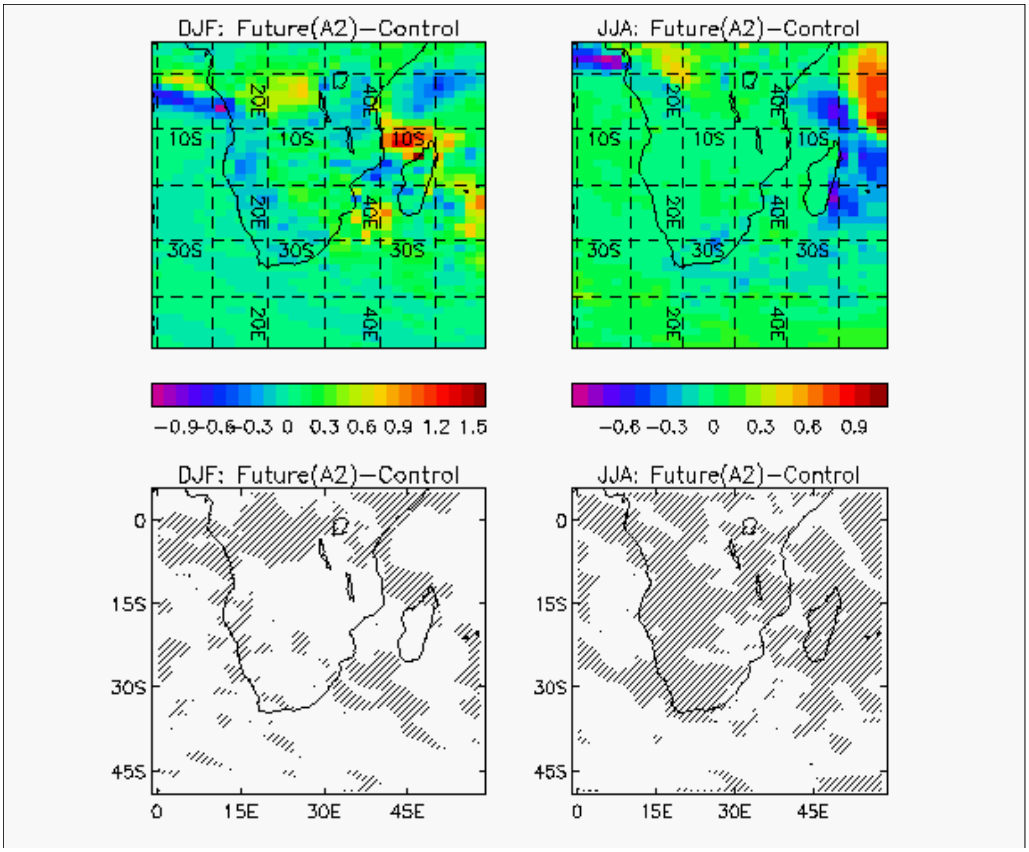

Figure 33: Thirty-year mean difference between the interannual variability of seasonal mean precipitation (mm/day) simulated by the SRES A2 scenario and control simulations for December to February (DJF) and June to August (JJA). The shading in the lower diagrams show statistically significant changes at the 5% significance level (F-test).

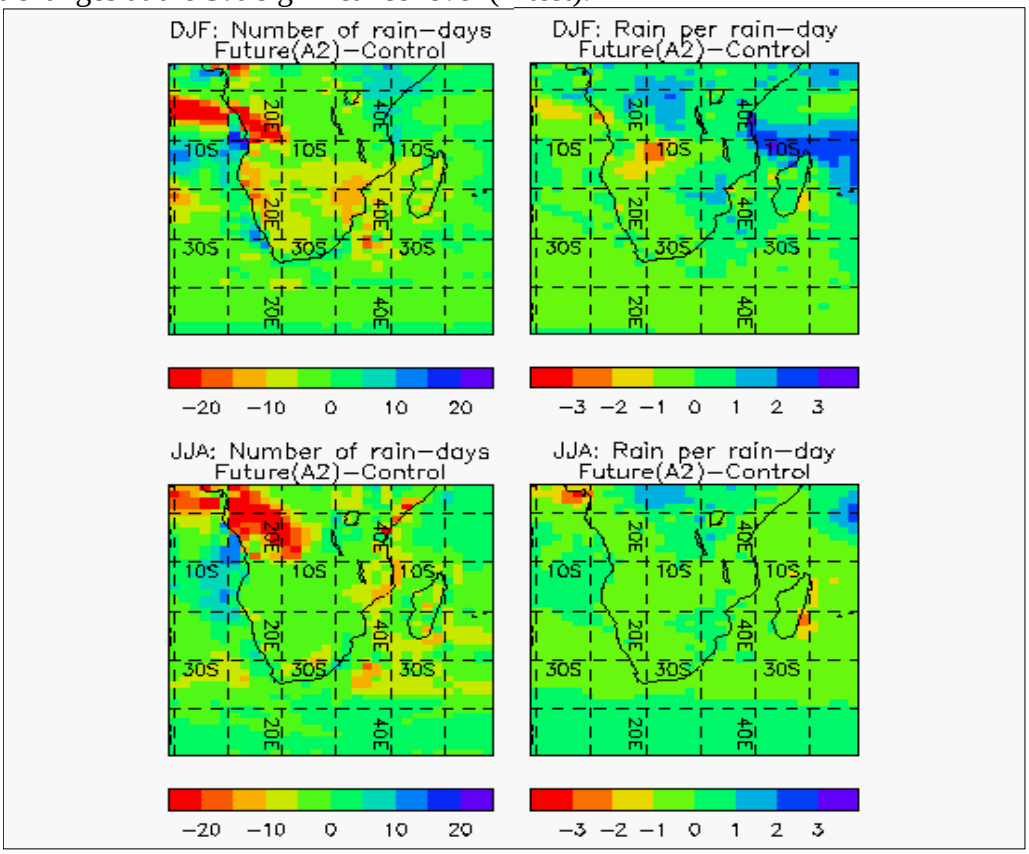

Figure 34: Thirty-year mean difference between the average number of rain-days and the rain per rain-day (mm) respectively, simulated by the SRES A2 scenario and control simulations for December to February (DJF) and June to August (JJA).

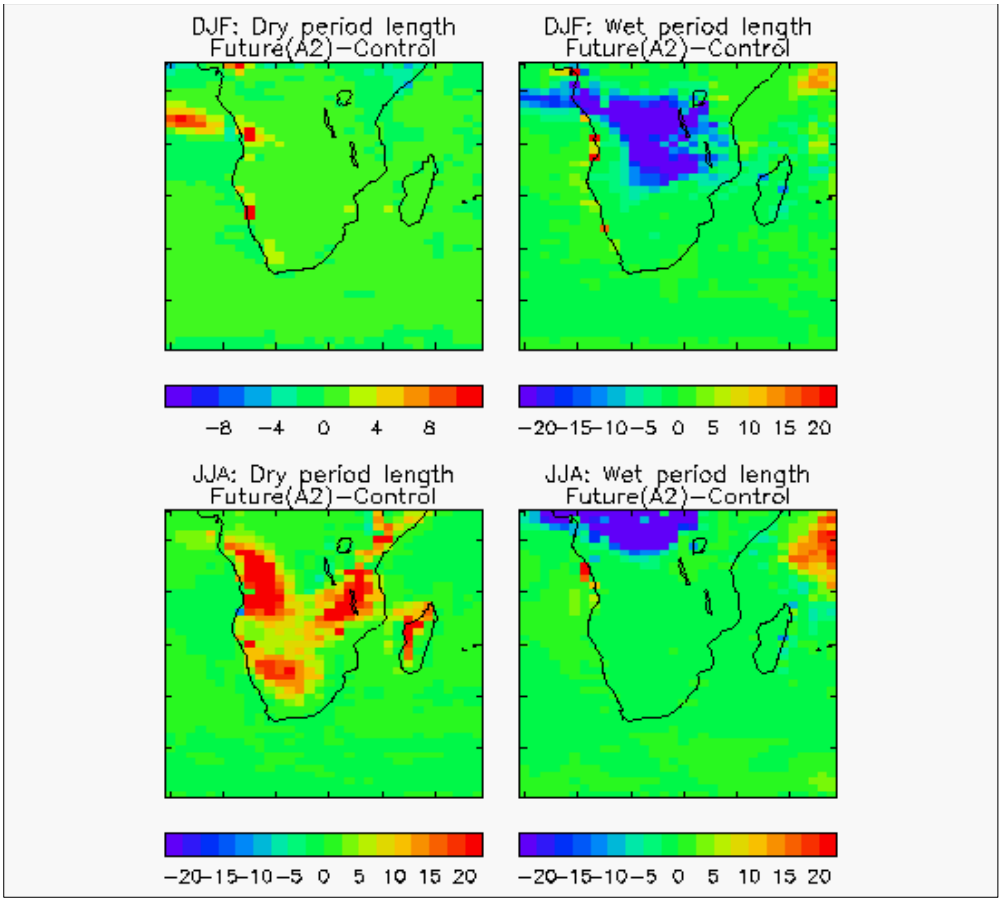

Figure 35: Thirty-year mean difference between the average number of consecutive dry days (dry period length) and consecutive wet days (wet period length) respectively, simulated by the SRES A2 scenario and control simulations for December to February (DJF) and June to August (JJA).

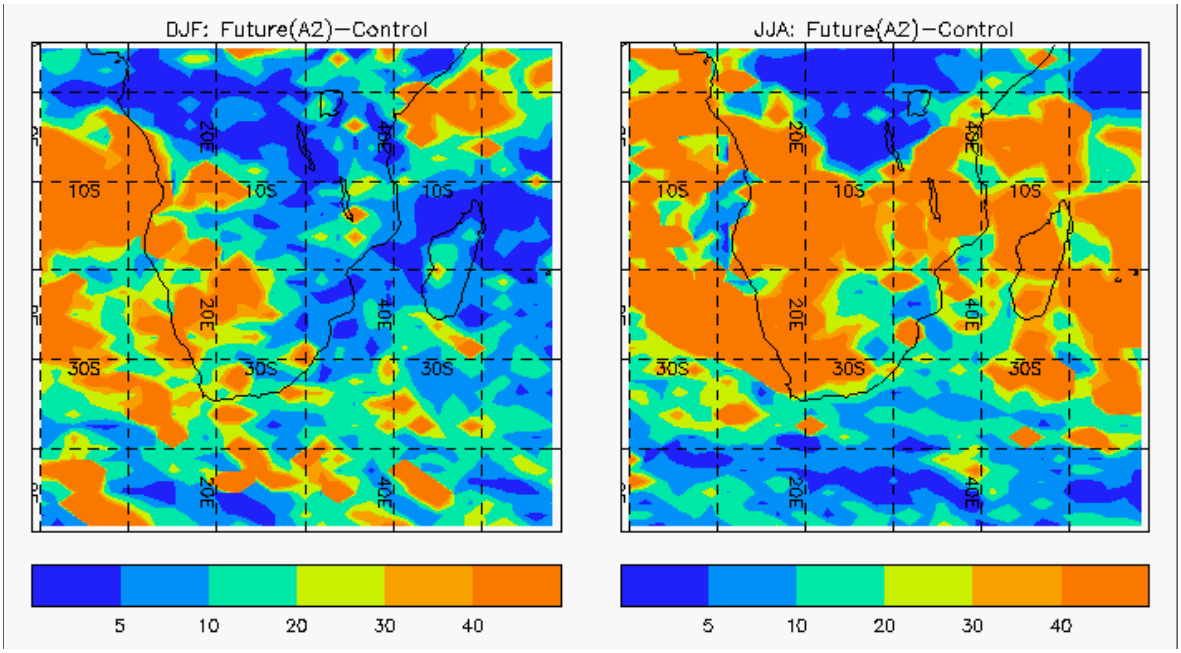

Figure 36: Return periods in the A2 scenario which are associated with the control simulation 20-year return values for December to February (DJF) and June to August (JJA).

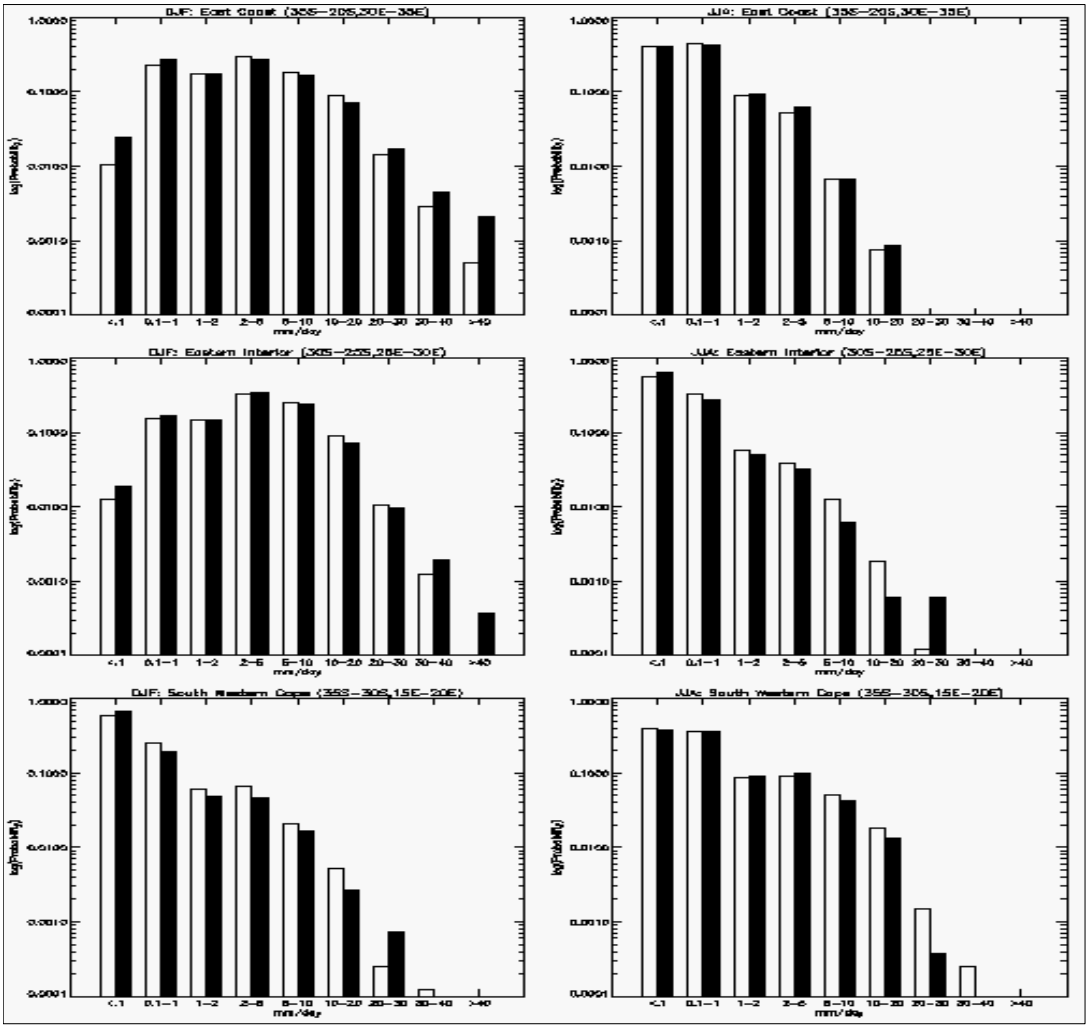

Figure 37: Histograms of the estimated probability (log scale) of rainfall (mm/day) falling in different classes for three regions of South Africa from the control simulations (open bars) and the A2 scenario simulations (solid bars) for December to February (DJF) and June to August (JJA).